Japan) and 82 gliomas were collected at collaborating hospitals. The study was approved by the Ethics Committee of the University of Tokyo and all patients gave written informed consent. Histological diagnoses were made on formalin-fixed, paraffin-embedded tissues following the WHO classification[1] by a neuropathologist (J.S.) for samples from the University of Tokyo hospital and consensus diagnoses were made by four neuropathologists for samples from other hospitals as reported previously.[23] Genomic DNA was extracted for genetic analyses. Patients with the same grade (2, 3, or 4) glioma were treated similarly with surgical resection followed by radiotherapy and alkylating agent chemotherapy.

Genetic analysis. For *IDH* gene mutations, the genomic regions spanning the catalytic domain of *IDH1*, including codon 132, and of *IDH2*, including codon 172, were analyzed by direct sequencing using the Genetic Analyzer 310 (Applied Biosystems, Foster City, CA, USA). An aliquot of DNA was amplified by PCR using AmpliTaq Gold (Applied Biosystems) with annealing temperature at 55°C. The primers 5′-TGCCACCAACGACCAAGTCA and 5′-TGTGTTGAGATGGACGCCTATTTG were used for *IDH1* amplification and sequencing, as reported previously.[15] Amplification of *IDH2* was carried out using the primers 5′-CTCTGTCCTCACAGAGTTCAAGC and 5′-CCACTCCTTGACACCACTGCC, and the *IDH2* sequencing reactions were carried out using the primers 5′-AAGTCCCAATGGAACTATCCG and 5′-TCTGTGGCCTTGTACTGCAGAG.

Loss of heterozygosity on chromosomes 1p and 19q was determined using microsatellite analysis as described previously.[23] When tumors had no available paired blood DNA or when the LOH assay was ambiguous because of non-informative microsatellite markers, MLPA assay was carried out using the SALSA MLPA kit P088 (MRC Holland, Amsterdam, the Netherlands) following the manufacturer's instructions. *TP53* gene mutation was determined by direct sequencing following PCR-SSCP screening of exons 5–8 of *TP53*, as described previously.[24]

Methylation-specific PCR. Genomic DNA samples (250 ng each) were used for bisulfite reactions using the EZ DNA Methylation Kit (Zymo Research, Irvine, CA, USA) according to the manufacturer's protocol. DNA methylation status of the *MGMT* promoter was then determined by methylation-specific PCR as described by Esteller *et al.*[25]

Statistical analysis. Fisher's exact test was used to compare the genotype distributions. Overall survival was defined as the time between initial surgery and death or last follow-up. Progression-free survival was defined as the time between initial surgery and recurrence or last follow-up. Both OS and PFS were calculated according to the Kaplan–Meier method, and differences among patient subsets were evaluated using the log–rank test. Statistical calculations were carried out using JMP 9 (SAS Institute, Cary, NC, USA).

Results

Frequency and characteristics of *IDH* mutations in glioma samples from Japanese patients. We analyzed 250 human glioma samples obtained following surgery; these tumors consisted of 125 GBM, 29 AA, 29 DA, 52 oligodendroglial tumors, 9 PA, and 6 GGL. Mutations of *IDH1* and *IDH2* were found in 73 (29%) and 2 (1%) tumors, respectively. All detected mutations were heterozygous, missense mutations. Among the 73 *IDH1* mutations, the G395A (R132H) substitution was the most frequent mutation (occurring in 70/73 cases, 96%), C394A (R132S) substitutions occurred in two cases, and a C394T (R132C) substitution occurred in one case. Of the two *IDH2* mutations, one was a G515A (R172K) substitution, and the other was an A514T (R172W) substitution. *IDH* mutations (*IDH1* or *IDH2*) were found in 13 (10%) of 125 GBM, 8 (28%) AA, 17 (59%) DA, and in 37 (71%) oligodendroglial tumors (Table 1). In the 52 oligodendroglial tumors, *IDH* mutations were found in 19/25 (76%) OG, 4/7 (57%) OA, 10/15 (67%) AOG, and 4/5 (80%) AOA. No mutation was detected in any case of PA or GGL. A higher rate of *IDH* mutation was found in secondary GBM (6/13, 46%) than primary GBM (6/109, 6%). In the three GBMO cases, there was only one *IDH1* mutation.

Association between *IDH* mutation and 1p/19q co-deletion, *TP53* mutation, or *MGMT* promoter methylation. The frequencies of 1p/19q co-deletion and *TP53* mutation and their relationship with *IDH* mutations are shown in Table 1. As expected, 1p/19q co-deletion was common in oligodendroglial tumors, especially those without an astrocytic component (OG 76%, AOG 67%), whereas *TP53* mutations were common in lower-grade astrocytomas (DA 45%); these genetic aberrations were never coincident. In OG, 1p/19q co-deletion was significantly correlated with *IDH* mutation ($P < 0.001$), and almost all oligodendroglial tumors with 1p/19q co-deletion had an *IDH* mutation (28/30, 93%).

The *TP53* mutation was more prevalent in DA (45%) than in AA (34%) or primary GBM (22%). However, when *IDH* mutation was present, *TP53* mutation was more frequent, and *TP53* mutations were found in 12/17 (71%) DA, 5/8 (63%) AA, and 3/6 (50%) primary GBMs that also had an *IDH* mutation. The rates of *IDH* mutation in astrocytic tumors with *TP53* mutation were higher than those with wild-type *TP53* (92% *vs* 31% in DA, 50% *vs* 16% in AA, and 13% *vs* 4% in primary GBM), and the association between *TP53* and *IDH* mutation was significant in DA ($P = 0.0018$), but not in AA or GBM. The majority of DA tumors with *TP53* mutation had *IDH* mutation (12/13, 92%); in contrast, only a few primary GBM tumors with *TP53* mutation also had an *IDH* mutation (3/23, 13%).

Of a total 250 gliomas, *MGMT* promoter methylation status was analyzed for 132 gliomas (grade 2, 3, and 4) resected at the University of Tokyo hospital. Methylation was evident in 37/69 GBM (54%), 5/18 AA (28%), 10/17 DA (59%), 8/10 AOG/AOA (80%), and 13/18 OG/OA (72%) (Table 1). The association between *IDH* mutation and *MGMT* methylation was significant in grade 2 ($P < 0.001$) and grade 3 gliomas ($P = 0.02$), but not in grade 4 gliomas ($P = 0.11$).

Prognostic value of *IDH* mutation and other genetic alterations. We evaluated the potential prognostic value of *IDH* mutation and other genetic alterations in WHO grade 2, 3, and 4 gliomas. For patients with grade 2 gliomas, univariate analysis showed that *IDH* mutation was not associated with OS ($P = 0.07$) or PFS ($P = 0.29$). Codeleted 1p/19q and wild-type *TP53* each slightly correlated with increased PFS ($P = 0.014$ and $P = 0.029$, respectively), but they were not correlated with OS, and neither of these genetic alterations showed significant association with prognosis in multivariate analysis (Table 2). *MGMT* promoter methylation was also not associated with prognosis. Similarly, we did not observe a significant association of *IDH* mutation with better prognosis for DA (OS, $P = 0.10$; PFS, $P = 0.58$).

In grade 3 gliomas, univariate analysis showed that the association between *IDH* mutation and prolonged survival (OS, $P = 0.0004$; PFS, $P < 0.0001$) was significant and that 1p/19q co-deletion was associated with prolonged survival (OS, $P = 0.028$; PFS, $P = 0.0025$), but that neither *TP53* mutation nor *MGMT* promoter status was associated with prognosis. Although *IDH* mutation and 1p/19q co-deletion were tightly associated with one another, the multivariate analysis further indicated that these alterations were independent indicators of a favorable prognosis (Table 2). *IDH* mutation was present in almost all tumors with the 1p/19q co-deletion.[26] Therefore, grade 3 gliomas were divided into three genetic subgroups: (i) 1p/19q codeleted tumors, most of which carry *IDH* mutation and show oligodendroglial phenotype; (ii) tumors without 1p/19q co-deletion and with mutant *IDH*; and (iii) tumors

doi: 10.1111/j.1349-7006.2011.02175.x

Table 1. *IDH* mutation and common genetic and epigenetic alterations in gliomas from Japanese patients

Tumor pathology (WHO grade) *IDH1* or *IDH2* status	No. of patients	Frequency of *IDH1* or *IDH2* mutation	Median age, years	Male sex (%)	1p/19q co-deletion	*TP53* mutation	Methylated *MGMT* promoter (%)
GBM primary (Gr. 4)	109	6/109 (6%)	62	61	1	23 (22%)	27/57 (47)
Mutant	6		43	50	1	3 n.s.	1/1 (100)
Wild-type	103		62	61	0	20	26/56 (46)
GBM secondary (Gr. 4)	13	6/13 (46%)	47	69	0	2 (15%)	7/9 (78)
Mutant	6		52	50	0	2 n.s.	4/5 (80)
Wild-type	7		43	86	0	0	3/4 (75)
GBMO (Gr.4)	3	1/3 (33%)	80	67	1	0	3/3 (100)
Mutant	1		62	100	1	0	1/1 (100)
Wild-type	2		80	50	0	0	2/2 (100)
Anaplastic astrocytoma (Gr. 3)	29	8/29 (28%)	57	55	1	10 (34%)	5/18 (28)
Mutant	8		46	50	1	5 n.s.	2/5 (40)
Wild-type	22		60	57	0	5	3/13 (23)
Anaplastic oligoastrocytoma (Gr. 3)	5	4/5 (80%)	43	40	0	4 (80%)	2/3 (66)
Mutant	4		48	25	0	3 n.s.	2/2 (100)
Wild-type	1		11	100	0	1	0/1 (0)
Anaplastic oligodendroglioma (Gr. 3)	15	10/15 (67%)	62	56	10 (67%)	0	6/7 (86)
Mutant	10		49	43	9*	0	5/5 (100)
Wild-type	5		66	100	1	0	1/2 (50)
Diffuse astrocytoma (Gr. 2)	29	17/29 (59%)	32	61	3	13 (45%)	10/17 (59)
Mutant	17		33	59	2	12***	10/10 (100)
Wild-type	12		30	64	1	1	0/7 (0)
Oligoastrocytoma (Gr. 2)	7	4/7 (57%)	44	71	1	1	5/6 (83)
Mutant	4		37	100	1	1	3/3 (100)
Wild-type	3		53	33	0	0	2/3 (67)
Oligodendroglioma (Gr. 2)	25	19/25 (76%)	46	52	19 (76%)	3	8/12 (66)
Mutant	19		47	53	18**	1	7/10 (70)
Wild-type	6		34	50	1	2	1/2 (50)
Pilocytic astrocytoma (Gr. 1)	9	0%	12	56	0	0	N/A
Mutant	0		N/A	N/A	0	0	
Wild-type	9		12	56	0	0	
Ganglioglioma (Gr. 1)	6	0%	22	67	0	0	N/A
Mutant	0		N/A	N/A	0	0	
Wild-type	6		22	67	0	0	

*$P = 0.0037$; **$P = 0.0001$; ***$P = 0.0018$. The association with *IDH* mutation (Fisher's exact test). GBM, glioblastoma; GBMO, glioblastoma with oligodendroglioma component; N/A, not analyzed; n.s., not significant.

Table 2. Prognostic value of common genetic alterations for overall survival (OS) and progression-free survival (PFS) in gliomas (multivariate analysis)

	PFS			OS		
	P-value	Hazard ratio	95% CI	*P*-value	Hazard ratio	95% CI
Grade 2 glioma						
IDH mutation	0.4408	0.602	0.1678–2.1535	0.1573	0.329	0.0728–1.5270
1p/19q co-deletion	0.3591	0.495	0.1083–2.2020	0.7988	1.237	0.2353–6.0194
TP53 mutation	0.2904	2.036	0.5526–7.7157	0.4693	0.537	0.0685–2.6350
Grade 3 glioma						
IDH mutation	<0.0001†	0.059	0.0086–0.2395	0.0403†	0.319	0.0985–0.9519
1p/19q co-deletion	0.0016†	0.055	0.0025–0.3904	0.0170†	0.184	0.0271–0.7567
TP53 mutation	0.4144	0.646	0.2045–1.7994	0.0300†	0.294	0.0786–0.8937
Primary GBM						
IDH mutation	0.8456	0.898	0.2575–2.4255	0.8560	0.905	0.2609–2.4203
TP53 mutation	0.1533	0.605	0.2792–1.1944	0.3089	0.705	0.3354–1.3613
Methylated *MGMT* promoter	0.0031†	0.407	0.2216–0.7375	0.0058†	0.429	0.2324–0.7820

†Significant value. Cox proportional hazard modeling for OS or PFS was applied for the major variable for prognostic factors. CI, confidence interval; GBM, glioblastoma.

without 1p/19q co-deletion and with wild-type *IDH*. Grade 3 gliomas were assessed with regard to the association between the genetic alterations and disease course (Fig. 1). In these genetic subgroups, grade 3 gliomas without 1p/19q co-deletion and with wild-type *IDH* were revealed to have markedly worse OS ($P < 0.0001$) (Fig. 1C) and PFS ($P < 0.0001$) (Fig. 1D), but

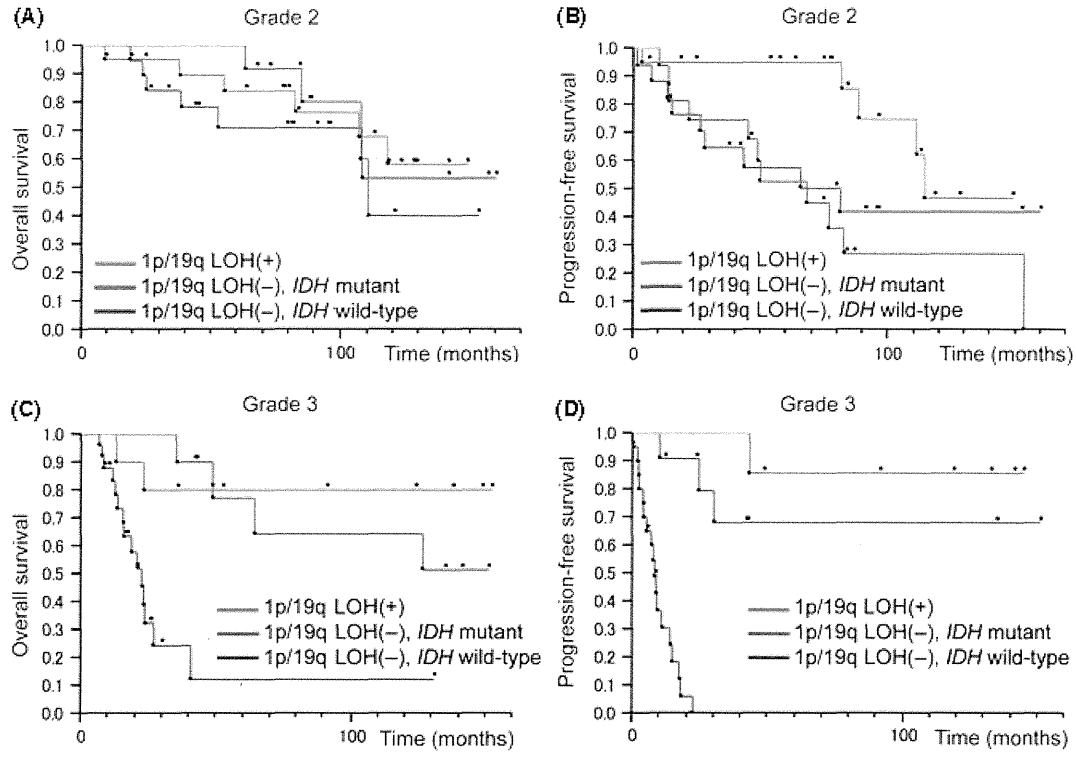

Fig. 1. Overall survival (OS) and progression-free survival (PFS) curves for patients with grade 2 and 3 gliomas with or without 1p/19q loss of heterozygosity (LOH) and/or isocitrate dehydrogenase (*IDH*) mutation. Overall survival (A) and PFS (B) in grade 2 gliomas; OS (C) and PFS (D) in grade 3 gliomas.

these lower survival rates were not observed for patients with grade 2 gliomas lacking 1p/19q co-deletion and *IDH* mutation (Fig. 1A,B). Grade 3 gliomas without 1p/19q co-deletion were predominantly AA (28 AAs, 5 AOAs, and 5 AOGs), and only 1 AA had the 1p/19q co-deletion (Table 1). The *IDH* mutation was significantly associated with increased OS ($P = 0.0064$) and PFS ($P = 0.0001$) for patients with AA based on the univariate analysis. *TP53* mutation was also correlated with increased PFS ($P = 0.013$), but *MGMT* promoter methylation showed no significant association with PFS or OS.

In primary GBM, our univariate analysis showed that neither *IDH* mutation, 1p/19q co-deletion, nor *TP53* mutation was associated with PFS or OS, but *MGMT* promoter methylation was significantly associated with increased OS ($P = 0.0043$) and PFS ($P = 0.0038$).

Discussion

Here we report that *IDH* mutation, which was tightly associated with 1p/19q co-deletion and *MGMT* promoter methylation, was common in grade 2 gliomas and also, but to a lesser extent, in grade 3 gliomas. Moreover, we found that *IDH* mutation would be an especially useful genetic marker for evaluating the malignancy of grade 3 gliomas that do not have a 1p/19q co-deletion and that these gliomas were predominantly AA.

The frequencies and patterns of *IDH* mutation in our glioma samples from Japanese patients were largely comparable to those in previous reports.[2–7] *IDH* mutation was found predominantly in grade 2 glioma, such as DA, OA, and OG. *IDH* mutation frequencies were lower in higher-grade gliomas, and less than 10% of GBM had an *IDH* mutation; however, nearly half of secondary GBM, which developed from malignant transformation of lower-grade glioma, had an *IDH* mutation. These observations supported the notion that the *IDH* mutation has a crucial role in the development of the majority of grade 2 gliomas. In grade 3 gliomas, the oligodendroglial tumors had higher frequency of *IDH* mutation than astrocytic tumors (OG 76% > DA 59%, $P = 0.18$; AOG 67% > AA 28%, $P < 0.05$; Pearson's chi-square-test). No *IDH* mutation was detected in any grade 1 glioma, PA or GGL; this observation indicated that these tumors had a different genetic etiology from that of grade 2 and 3 infiltrative astrocytic and oligodendroglial tumors. This observation also supported the usefulness of *IDH* mutations along with BRAF alterations for differential diagnosis of PA.[27] However, our results differed from two previous reports that detected *IDH1* mutation (8–38%) in GGL.[5,28] Further studies are needed to clarify the biological and clinical significance of *IDH1* mutation in GGL.

As reported previously,[23] *TP53* mutation and co-deletion of chromosomes 1p and 19q were frequent alterations in grade 2 and grade 3 gliomas. The 1p/19q co-deletions were mostly found in oligodendroglial lineage gliomas, whereas *TP53* mutations were more frequent in gliomas derived from the astrocytic lineage. *IDH* mutation is currently believed to precede 1p/19q LOH and *TP53* mutation during the early stage of gliomagenesis,[4,6] and consistent with this hypothesis, most of our grade 2 gliomas that had 1p/19q co-deletion or *TP53* mutations also harbored an *IDH* mutation. In one study, all the gliomas with deletions of the entire 1p and 19q arms carried an *IDH1* or *IDH2* mutation;[26] however, we found a few exceptions in which there was 1p/19q LOH, but no *IDH* mutation. These apparent exceptions might have been artifacts due to our imperfect methods for detecting the extent of 1p/19q LOH, specifically microsatellite analysis or MLPA; these methods do not effectively differentiate partial chromosomal loss from typical entire 1p/19q hemizygous deletion, which is generally found in OG harboring *IDH* mutation. It would be better to carefully evaluate the extent of 1p/19q LOH in such exceptional cases. *TP53* mutation was also

doi: 10.1111/j.1349-7006.2011.02175.x

associated with *IDH* mutation in DA. However, there was no association between *IDH* and *TP53* mutation in AA or primary GBM. This observation suggested that *TP53* mutation promoted tumor growth independently of *IDH* mutation, especially in higher grade gliomas. Most gliomas with an *IDH* mutation had either 1p/19q LOH or *TP53* mutation, further supporting the hypothesis that combinations of *IDH* mutation and subsequent genetic alteration are common pathways leading to low-grade glioma. However, there were also a few other *IDH*-mutated gliomas that had neither 1p/19q co-deletion nor *TP53* mutation. In these gliomas, the kind of alterations subsequent to *IDH* mutation that caused progenitor cells to give rise to low-grade glioma remains to be elucidated.

Methylation at the *MGMT* promoter was associated with *IDH* mutation, especially for low-grade gliomas. Some IDH enzymes with a mutation in the catalytic domain acquire a novel enzymatic activity[9,11] that causes accumulation of 2-HG, and 2-HG is known to inhibit enzymes such as 5-methylcytosine hydroxylases and histone demethylases. As a result, *IDH* mutations bring about genome-wide hypermethylation, which might lead to tumor initiation.[12,29] Reportedly, the majority of low-grade gliomas have hypermethylated CpG islands throughout the genome; this phenomenon is called the glioma CpG island methylator phenotype, and these tumors frequently harbor *IDH* mutation.[30–32] Therefore, frequent *MGMT* promoter methylation in *IDH*-mutated low-grade glioma was possibly simply a reflection of hypermethylation of a plethora of genes resulting from the methylator phenotype. In contrast, the majority of GBM had *MGMT* promoter hypermethylation without also having *IDH* mutation, indicating that *MGMT* promoter methylation occurs independent of *IDH*-related hypermethylation in most GBM. Probably because of such a background, the prognostic values of *MGMT* promoter methylation for *IDH*-mutated and *IDH*-wild-type gliomas are not equal. In GBM, *MGMT* promoter methylation is a predictive factor for the efficacy of temozolomide, which is a common alkylating agent used in the chemotherapeutic treatment of malignant glioma.[33,34] However, the predictive value of *MGMT* promoter methylation for chemosensitivity in grade 2 and grade 3 glioma is controversial.[19,35]

The prognostic significance of *IDH* mutation differed among WHO tumor grades. Unlike previous reports, *IDH* mutation was not associated with the PFS or OS of our GBM patients; however, this finding might result from insufficient numbers of GBM patients with *IDH* mutation. A methylated *MGMT* promoter, which reflects the sensitivity of a tumor to temozolomide, was associated with favorable PFS and OS for patients with GBM, further emphasizing the importance of detecting *MGMT* promoter methylation status in GBM.

Among patients with grade 2 gliomas, *IDH* mutation was also not associated with prognosis. Wild-type *TP53* and 1p/19q co-deletion were each associated with prolonged PFS, probably because these two genetic alterations were mutually exclusive and tumors with wild-type *TP53* likely have a 1p/19q co-deletion, which is a recognized favorable prognostic factor. The prognostic value and predictability of temozolomide efficacy associated with *IDH* mutation in low-grade gliomas has been controversial. Consistent with our results, Kim *et al.*[20] showed that *IDH1* and *IDH2* mutations are not prognostic in low-grade gliomas, but that *TP53* mutation is a significant prognostic indicator of shorter survival and 1p/19q loss is prognostic of longer survival. However, Sanson *et al.*[15] reported a different result, specifically that *IDH1* mutation is associated with a better outcome in grade 2 gliomas. Dubbink *et al.*[18] showed that *IDH* mutation is associated with better outcomes for relapsed astrocytomas previously treated with radiotherapy, but there was no relationship between *IDH* mutation and temozolomide responsiveness. Houillier *et al.*[19] showed that *IDH1* or *IDH2* mutations predict better prognosis of glioma treated with temozolomide, but they did not appear to influence the course of untreated low-grade glioma. Thus, the prognostic value of *IDH* mutation is different from that of 1p/19q co-deletion, which is prognostic as well as predictive for responsiveness to temozolomide in low-grade gliomas. These inconsistent results on the association between *IDH* mutation and survival in cases of low-grade gliomas might be caused by the variable numbers of OG and DA included in these studies. Almost all oligodendroglial tumors with 1p/19q co-deletion also have an *IDH* mutation;[26] therefore, many cases of OG with favorable prognoses may affect and confound measurements of survival rate in the whole group of low-grade gliomas with *IDH* mutations. To avoid the confounding influence of OG, we also focused on DA with wild-type *IDH*; these tumors generally have neither 1p/19q LOH nor *TP53*. However, they had outcomes comparable to those of DA with *IDH* mutation. This finding indicated that DA with wild-type *IDH* was not more malignant than DA with an *IDH* mutation. This observation differed from the observation that AA with wild-type *IDH* had markedly worse outcomes than AA with an *IDH* mutation (OS, $P = 0.0064$; PFS, $P = 0.0001$).

In contrast with grade 2 and 4 gliomas, the prognostic significance of *IDH* mutation was evident for grade 3 gliomas, and this finding was consistent with previous reports.[15,17,36] Almost all gliomas with 1p/19q co-deletion have an *IDH* mutation,[26] and anaplastic oligodendroglial tumors often harbor 1p/19q co-deletion; therefore, monitoring of *IDH* mutation might have more clinical significance for patients with grade 3 gliomas with intact 1p/19q, and these tumors are predominantly AA. In fact, as the histopathological differential diagnosis of AA from GBM or DA is often subjective and diagnoses frequently differ between pathologists,[23] a pathological diagnosis of AA may not always indicate sameness between gliomas and similar prognosis. However, accurate determination of the pathological group of a tumor is clinically critical for planning adjuvant therapy, such as radiation and chemotherapy. Therefore, genetic analyses, which may reflect causative origins of tumors, are expected to reveal biological traits with less inter-observer variation, as is the case of 1p/19q co-deletion in oligodendroglial tumors. Because *IDH* mutations have a defined role in gliomagenesis and indicate, to some extent, the nature of the original tumor cell, monitoring *IDH* mutational status may allow for accurate assignment of diagnosed AA to low-grade gliomas that frequently harbor *IDH* mutation or to primary GBM that usually have intact *IDH*. Therefore, we believe that monitoring *IDH* mutation in combination with 1p/19q co-deletion, which genetically differentiates oligodendroglial and astrocytic tumors, could be a useful genetic marker of prognostic value, especially for grade 3 glioma patients.

Acknowledgments

We appreciate the technical assistance of Reiko Matsuura (Department of Neurosurgery, University of Tokyo, Tokyo, Japan). This work was supported in part by a Grant-in-Aid for Scientific Research (C) (No. 20591706) to A.M. and a Grant-in-Aid for Young Scientists (B) (No. 22791334) to K.S. from the Japan Society for the Promotion of Science. A.M. was also supported by the Takeda Science Foundation.

Disclosure Statement

The authors have no conflicts of interest.

Abbreviations

2-HG	2-hydroxyglutarate
AA	anaplastic astrocytoma
AOA	anaplastic oligoastrocytoma
AOG	anaplastic oligodendroglioma

DA	diffuse astrocytoma
GBM	glioblastoma
GBMO	glioblastoma with oligodendroglioma component
GGL	ganglioglioma
IDH	isocitrate dehydrogenase
LOH	loss of heterozygosity
MLPA	multiplex ligation-dependent probe amplification
OA	oligoastrocytoma
OG	oligodendroglioma
OS	overall survival
PA	pilocytic astrocytoma
PFS	progression-free survival

References

1 Louis DN, Ohgaki H, Wiestler OD, Cavenee WK, eds. *WHO Classification of Tumours of the Central Nervous System*, 4th edn. Lyon: International Agency for Research on Cancer, 2007.
2 Parsons DW, Jones S, Zhang X *et al.* An Integrated Genomic Analysis of Human Glioblastoma Multiforme. *Science* 2008; **321**: 1807–12.
3 Balss J, Meyer J, Mueller W, Korshunov A, Hartmann C, Deimling A. Analysis of the *IDH1* codon 132 mutation in brain tumors. *Acta Neuropathol (Berl)* 2008; **116**: 597–602.
4 Ichimura K, Pearson DM, Kocialkowski S *et al. IDH1* mutations are present in the majority of common adult gliomas but rare in primary glioblastomas. *Neuro Oncol* 2009; **11**: 341–7.
5 Sonoda Y, Kumabe T, Nakamura T *et al.* Analysis of *IDH1* and *IDH2* mutations in Japanese glioma patients. *Cancer Sci* 2009; **100**: 1996–8.
6 Watanabe T, Nobusawa S, Kleihues P, Ohgaki H. *IDH1* Mutations Are Early Events in the Development of Astrocytomas and Oligodendrogliomas. *Am J Pathol* 2009; **174**: 1149–53.
7 Yan H, Parsons DW, Jin G *et al. IDH1* and *IDH2* mutations in gliomas. *N Engl J Med* 2009; **360**: 765–73.
8 Mardis ER, Ding L, Dooling DJ *et al.* Recurring mutations found by sequencing an acute myeloid leukemia genome. *N Engl J Med* 2009; **361**: 1058–66.
9 Ward PS, Patel J, Wise DR *et al.* The Common Feature of Leukemia-Associated IDH1 and IDH2 Mutations Is a Neomorphic Enzyme Activity Converting α-Ketoglutarate to 2-Hydroxyglutarate. *Cancer Cell* 2010; **17**: 225–34.
10 Bleeker FE, Lamba S, Leenstra S *et al. IDH1* mutations at residue p.R132 ($IDH1^{R132}$) occur frequently in high-grade gliomas but not in other solid tumors. *Hum Mutat* 2009; **30**: 7–11.
11 Dang L, White DW, Gross S *et al.* Cancer-associated IDH1 mutations produce 2-hydroxyglutarate. *Nature* 2009; **462**: 739–44.
12 Xu W, Yang H, Liu Y *et al.* Oncometabolite 2-Hydroxyglutarate Is a Competitive Inhibitor of α-Ketoglutarate-Dependent Dioxygenases. *Cancer Cell* 2011; **19**: 17–30.
13 Lesniak M, Jin G, Reitman ZJ *et al.* 2-Hydroxyglutarate Production, but Not Dominant Negative Function, Is Conferred by Glioma-Derived NADP+-Dependent Isocitrate Dehydrogenase Mutations. *PLoS ONE* 2011; **6**: e16812.
14 Nobusawa S, Watanabe T, Kleihues P, Ohgaki H. *IDH1* Mutations as Molecular Signature and Predictive Factor of Secondary Glioblastomas. *Clin Cancer Res* 2009; **15**: 6002–7.
15 Sanson M, Marie Y, Paris S *et al.* Isocitrate Dehydrogenase 1 Codon 132 Mutation Is an Important Prognostic Biomarker in Gliomas. *J Clin Oncol* 2009; **27**: 4150–4.
16 Van den Bent MJ, Dubbink HJ, Marie Y *et al. IDH1* and *IDH2* Mutations Are Prognostic but not Predictive for Outcome in Anaplastic Oligodendroglial Tumors: a Report of the European Organization for Research and Treatment of Cancer Brain Tumor Group. *Clin Cancer Res* 2010; **16**: 1597–604.
17 Shibahara I, Sonoda Y, Kanamori M *et al. IDH1/2* gene status defines the prognosis and molecular profiles in patients with grade III gliomas. *Int J Clin Oncol* 2011; DOI: 10.1007/s10147-011-0323-2 [Epub ahead of print].
18 Dubbink HJ, Taal W, Van Marion R *et al. IDH1* mutations in low-grade astrocytomas predict survival but not response to temozolomide. *Neurology* 2009; **73**: 1792–5.
19 Houillier C, Wang X, Kaloshi G *et al. IDH1* or *IDH2* mutations predict longer survival and response to temozolomide in low-grade gliomas. *Neurology* 2010; **75**: 1560–6.
20 Kim Y-H, Nobusawa S, Mittelbronn M *et al.* Molecular Classification of Low-Grade Diffuse Gliomas. *Am J Pathol* 2010; **177**: 2708–14.
21 Jha P, Suri V, Sharma V *et al. IDH1* mutations in gliomas: first series from a tertiary care centre in India with comprehensive review of literature. *Exp Mol Pathol* 2011; **91**: 385–93.
22 Qi SA, Yu L, Lu YT *et al. IDH* mutations occur frequently in Chinese glioma patients and predict longer survival but not response to concomitant chemoradiotherapy in anaplastic gliomas. *Oncol Rep* 2011; **26**: 1479–85.
23 Ueki K, Nishikawa R, Nakazato Y *et al.* Correlation of histology and molecular genetic analysis of 1p, 19q, 10q, *TP53*, *EGFR*, *CDK4*, and *CDKN2A* in 91 astrocytic and oligodendroglial tumors. *Clin Cancer Res* 2002; **8**: 196–201.
24 Mukasa A, Ueki K, Matsumoto S *et al.* Distinction in gene expression profiles of oligodendrogliomas with and without allelic loss of 1p. *Oncogene* 2002; **21**: 3961–8.
25 Esteller M, Hamilton SR, Burger PC, Baylin SB, Herman JG. Inactivation of the DNA repair gene O6-methylguanine-DNA methyltransferase by promoter hypermethylation is a common event in primary human neoplasia. *Cancer Res* 1999; **59**: 793–7.
26 Labussiere M, Idbaih A, Wang XW *et al.* All the 1p19q codeleted gliomas are mutated on *IDH1* or *IDH2*. *Neurology* 2010; **74**: 1886–90.
27 Korshunov A, Meyer J, Capper D *et al.* Combined molecular analysis of *BRAF* and *IDH1* distinguishes pilocytic astrocytoma from diffuse astrocytoma. *Acta Neuropathol* 2009; **118**: 401–5.
28 Horbinski C, Kofler J, Yeaney G *et al.* Isocitrate dehydrogenase 1 analysis differentiates gangliogliomas from infiltrative gliomas. *Brain Pathol* 2011; **21**: 564–74.
29 Figueroa ME, Abdel-Wahab O, Lu C *et al.* Leukemic IDH1 and IDH2 Mutations Result in a Hypermethylation Phenotype, Disrupt TET2 Function, and Impair Hematopoietic Differentiation. *Cancer Cell* 2010; **18**: 553–67.
30 Christensen BC, Smith AA, Zheng S *et al.* DNA Methylation, Isocitrate Dehydrogenase Mutation, and Survival in Glioma. *J Natl Cancer Inst* 2010; **103**: 143–53.
31 Laffaire J, Everhard S, Idbaih A *et al.* Methylation profiling identifies 2 groups of gliomas according to their tumorigenesis. *Neuro Oncol* 2010; **13**: 84–98.
32 Noushmehr H, Weisenberger DJ, Diefes K *et al.* Identification of a CpG Island Methylator Phenotype that Defines a Distinct Subgroup of Glioma. *Cancer Cell* 2010; **17**: 510–22.
33 Hegi ME, Diserens AC, Gorlia T *et al. MGMT* gene silencing and benefit from temozolomide in glioblastoma. *N Engl J Med* 2005; **352**: 997–1003.
34 Rivera AL, Pelloski CE, Gilbert MR *et al.* MGMT promoter methylation is predictive of response to radiotherapy and prognostic in the absence of adjuvant alkylating chemotherapy for glioblastoma. *Neuro Oncol* 2010; **12**: 116–21.
35 Van den Bent MJ, Dubbink HJ, Sanson M *et al. MGMT* promoter methylation is prognostic but not predictive for outcome to adjuvant PCV chemotherapy in anaplastic oligodendroglial tumors: a report from EORTC Brain Tumor Group Study 26951. *J Clin Oncol* 2009; **27**: 5881–6.
36 Hartmann C, Hentschel B, Wick W *et al.* Patients with *IDH1* wild type anaplastic astrocytomas exhibit worse prognosis than *IDH1*-mutated glioblastomas, and *IDH1* mutation status accounts for the unfavorable prognostic effect of higher age: implications for classification of gliomas. *Acta Neuropathol (Berl)* 2010; **120**: 707–18.

doi: 10.1111/j.1349-7006.2011.02175.x

Journal of Radiation Research, 2013, 54, 61–69
doi: 10.1093/jrr/rrs078 Advance Access Publication 5 September 2012

In vitro stemness characterization of radio-resistant clones isolated from a medulloblastoma cell line ONS-76

Lue SUN[1], Takashi MORITAKE[2], Yun-Wen ZHENG[3], Kenshi SUZUKI[1], Ariungerel GERELCHULUUN[1], Zhengshan HONG[1], Junko ZENKOH[2], Hideki TANIGUCHI[3] and Koji TSUBOI[2,*]

[1]Graduate School of Comprehensive Human Sciences, University of Tsukuba, 1-1-1 Tennodai, Tsukuba, Ibaraki 305-8575, Japan
[2]Proton Medical Research Center, Faculty of Medicine, University of Tsukuba, 1-1-1 Tennodai, Tsukuba, Ibaraki 305-8575, Japan
[3]Department of Regenerative Medicine, Graduate School of Medicine, Yokohama City University, 3-9 Fukuura, Kanazawa-ku, Yokohama, Kanagawa 236-0004, Japan
*Corresponding author. Koji Tsuboi, Proton Medical Research Center, Graduate School of Comprehensive Human Sciences, University of Tsukuba, 1-1-1 Tennodai, Tsukuba, Ibaraki 305-8575, Japan.; E-mail: tsuboi-k@md.tsukuba.ac.jp; Tel: t81 29853 7100; Fax: t81 29853 7103.

(Received 28 May 2012; revised 27 July 2012)

One-third of patients with medulloblastoma die due to recurrence after various treatments including radiotherapy. Although it has been postulated that cancer stem-like cells are radio-resistant and play an important role in tumor recurrence, the "stemness" of medulloblastoma cells surviving irradiation has not yet been elucidated. Using a medulloblastoma cell line ONS-76, cells that survived gamma irradiation were investigated on their "stemness" *in vitro*. From 10 500 cells, 20 radio-resistant clones were selected after gamma ray irradiation (5 Gy × two fractions) using the replica micro-well technique. These 20 resistant clones were screened for CD133 positivity by flow cytometry followed by side population assay, tumor sphere formation assay and clonogenic survival assay. Results revealed CD133 fractions were significantly elevated in three clones, which also exhibited significantly increased levels of tumor sphere formation ability and side population fraction. Clonogenic survival assay demonstrated that their radio-resistance was significantly higher than the parental ONS-76. This may support the hypothesis that a small number of cancer stem-like cells (CSCs) are the main culprits in local recurrence after radiotherapy, and disruption of the resistance mechanism of these CSCs is a critical future issue in improving the outcome of patients with medulloblastoma.

Keywords: medulloblastoma; radiation; CD133; cancer stem-like cell

INTRODUCTION

Medulloblastoma is the most common pediatric central nervous system (CNS) tumor with an incidence of 0.5 per 100 000 children in Japan, and 0.65 per 100 000 in Europe [1]. Approximately 75% of medulloblastomas develop in the cerebellar vermis and it is most commonly seen at ages 6–7 years of age [1]. Although the current standard care for medulloblastoma consists of maximum surgical removal followed by conventional radiotherapy and concomitant chemotherapy [2–3], approximately one-third of patients die due to tumor recurrence [4]. Recurrence occurs not only because of the invasive and metastatic nature of the tumor [2], but also due to the restrictions on radiation doses to the CNS in children [5–7]. Another biological factor leading to treatment failure in one-third of patients may be tumor heterogeneity; a small mingled cell population survives chemo-radiotherapy and regenerates the tumor mass although most of the tumor cells are relatively sensitive to chemo-radiotherapy.

Recently, it has been suggested that the cancer stem-like cells (CSCs) are radio-resistant and may be involved in malignant brain tumor recurrence after radiotherapy [8–11]. Among these, CSCs in medulloblastoma have been reported

to be enriched in CD133-positive cells and to have tumor sphere formation ability [12–13]. In addition, it was reported that the side population fraction is closely related to the stemness of medulloblastoma cells through the Notch pathway [14]. Thus, to elucidate the mechanism of recurrence after chemo-radiotherapy in patients with medulloblastoma, it is essential to confirm that the medulloblastoma cells which survive irradiation contain radio-resistant CSCs.

Based on this background, we recreated the process of tumor recurrence after X-ray irradiation *in vitro* to prove the hypothesis that a small population of survivors is not only radio-resistant but also has the characteristics of CSCs.

MATERIALS AND METHODS

Cell line and culture condition

A human medulloblastoma cell line, ONS-76, was obtained from the RIKEN Cell Bank (Tsukuba, Ibaraki, Japan). ONS-76 was established from a primary culture of tumor tissue taken from a 2-year-old Japanese girl in 1987 [15]. It has been reported that ONS-76 possesses the neuronal cell markers neuron-specific enolase (NSE) and neurofilament protein (NFP) in the cytoplasm. Also, the ONS-76 line expresses class I and II major histocompatibility complex (MHC) following administration of interferon-gamma (IFN-γ). These phenomena suggest that ONS-76 can differentiate into both neural cells and glial cells; thus, ONS-76 may be kept in an undifferentiated or early differentiation state and may have neural stem cell-like properties [15]. Also, we have previously reported that ONS-76 cells form clear colonies with high plating efficiency [16], and a recent report defined that ONS-76 has wild-type p53 [17]. The cells were cultured in minimal essential medium (MEM) (Sigma-Aldrich Inc., Tokyo, Japan) containing 10% fetal bovine serum (FBS) (Nichirei Biosciences Inc., Tokyo, Japan), 100 mg/ml streptomycin and 100 U/ml penicillin (Sigma-Aldrich). The cells were incubated in a humidified atmosphere at 37°C with 5% CO_2 in the air. For subcultures, cells were rinsed with Ca^{2+} and Mg^{2+}-free phosphate buffered saline (PBS) (Sigma-Aldrich), and were dispersed with 0.25% trypsin containing 0.5 mM of ethylenediaminetetraacetate (EDTA) (Sigma-Aldrich).

Irradiation and dosimetry

ONS-76 cells in a logarithmic growing phase were irradiated with ^{137}cesium γ-rays at a dose rate of approximately 0.9 Gy/min using Gammacell (Atomic Energy, Ottawa, ON, Canada). Irradiation was performed at room temperature. Dosimetry at the same position was performed using a small chip photoluminescence glass dosimeter (PLD) system (Dose Ace; Asahi Techno Glass Co., Japan).

Isolation of surviving cells after irradiation

To isolate surviving clones after irradiation, the modified replica micro-well method was performed (Supplemental Fig. 1) [18]. First, ONS-76 cells in flasks were irradiated with 5 Gy of γ-rays. Then, the cells were trypsinized and suspended in MEM, and 350 cells were counted and seeded into thirty 10-cm dishes (Falcon, Becton Dickinson, Franklin Lakes, NJ, USA). After two weeks of incubation, the 96 largest colonies were selected and sampled by custom-made cloning cylinders, and transferred to three identical 96-well plates (Falcon, Becton Dickinson). After incubation for 24 h, one of the three plates was irradiated with 5 Gy of γ-rays again and the three plates were incubated for another 5 days. Finally, the cells in the irradiated plate and one of two unirradiated plates were fixed and stained with 0.25% methylene blue (Wako Pure Chemical Industries Ltd, Osaka, Japan) in 90% ethanol solution. Comparing the two stained plates macroscopically, the deep-colored candidates were selected and harvested from the corresponding wells of the remaining plate.

Immunocytochemistry by flow cytometry

The cells were detached by 0.25% trypsin-EDTA, and washed in PBS containing 2% FBS. Then, 2×10^6 cells were suspended in 80 μl of PBS with 2% FBS, and 20 μl of FcR blocking reagent (Miltenyi Biotec Inc., Tokyo, Japan) and 10 μl of anti-human CD133/1 mouse IgG1 antibody conjugated to phycoerythrin (PE) was added (Miltenyi Biotec). PE-labeled mouse IgG1 (BD Biosciences, Franklin Lakes, NJ, USA) was used as an isotype control. The cell suspension supplemented with these antibodies was incubated at 4°C in the dark. After 30 min of incubation, the cells were washed twice in PBS containing 2% FBS, and then propidium iodide (PI) (Sigma-Aldrich) was added at a final concentration of 1 μg/ml to eliminate dead cells. The treated cells were filtered through a 35-μm cell strainer before flow cytometry (BD FACSCalibur; BD Biosciences).

Tumor sphere limiting dilution assay

For limiting dilution assay, ONS-76 cells were dissociated with 0.25% trypsin-EDTA and suspended in PBS containing 2% FBS. Then, PI was added at a final concentration of 1 μg/ml, and PI-negative cells were sorted by MoFlo (Beckman Coulter Inc., Brea, CA, USA). The selected cells were counted and plated at numbers of 2, 5, 8, 10 and 20 cells per well of the ultra low attachment surface 96-well (Corning Inc., Lowell, MA, USA). The numbers of the cells were plated in 12 wells each of which contained 200 μl of serum-free medium (SFM) composed of Dulbecco's Modified Eagle Medium/Nutrient Mixture F-12 (DMEM/F12) medium (GIBCO, Life Technologies, Carlsbad, CA, USA), 20 ng/ml epidermal growth factor (EGF) (Sigma-Aldrich), 20 ng/ml basic fibroblast growth factor (bFGF)

(Sigma-Aldrich) and 20 μl/ml B27 supplement (GIBCO, Life Technologies). During incubation, the cells in the wells were fed with 0.025 ml of SFM on Days 2, 4 and 6. Finally, wells that did not contain spheres were selected macroscopically and their numbers counted on Day 7. The percentage of wells without tumor spheres was calculated and plotted against the number of cells plated per well. From the regression curves, x-intercept values were extrapolated to represent the number of cells required to form at least one tumor sphere in each clone.

Side population analysis

The cells were trypsinized, washed and resuspended at 10^6 cells/ml in Hank's balanced salt solution (HBSS) (Lonza Walkersville Inc., Walkersville, MD, USA) containing 3% FBS and 10 mM HEPES (GIBCO, Life Technologies). Then, Hoechst 33342 (Dojindo, Kumamoto, Japan) was added at a final concentration of 8 μg/ml with or without 15 μM reserpine (Sigma-Aldrich). Reserpine was used here because it is an adenosine-triphosphate (ATP)-binding cassette (ABC) transporters antagonist. It has been used to evaluate or confirm the presence of side-populations as it is able to selectively extinguish side-populations by its specific function [19]. After incubation at 37°C/5% CO_2 for 90 min with gentle agitation every 30 min, cells were washed twice with ice-cold HBSS containing 3% FBS and 10 mM HEPES, followed by and addition of PI to a final concentration of 1 μg/ml. Finally, the cells were filtered through a 35-μm cell strainer (Falcon, Becton Dickinson) to obtain single-cell suspensions, and placed on ice until analysis.

Aliquots of 5×10^5 or more cells were analyzed by MoFlo (Beckman Coulter). The Hoechst 33342 dye was excited by a 350-nm laser, and subjected to dual-wavelength analysis using a 457/50 (Hoechst blue) band-pass filter and 670/30 band-pass filter (Hoechst red). The PI was excited with a 488-nm laser and measured through the 670/30 band-pass filter for discrimination of dead cells.

Clonogenic survival assay

The cells in flasks were exposed to γ-rays with dose values of 1, 2, 4, 6, 8 and 10 Gy. After irradiation, the cells were trypsinized and counted, and the predetermined number of cells was plated onto five 60-mm dishes (Falcon, Becton Dickinson) at each dose point. After 14 days incubation, the colonies were fixed and stained with methylene blue solution 0.25% methylene blue (Wako Pure Chemical Industries) in 90% ethanol solution. The number of surviving colonies that include 50 cells or more was counted and averaged [20]. The survival curves were fitted to the linear-quadratic (LQ) model using DeltaGraph v.5.4 software (RedRock Software, Inc., Salt Lake City, UT, USA) as previously described [16].

Growth pattern and CD133-positive cell fraction analysis

The growth rates and CD133 positivity were analyzed simultaneously. Before the experiment, 1×10^6 cells were plated in T75 flasks (NUNC) and pre-incubated for 3 days. Then the cells were trypsinized and plated at a density of 1×10^6 cells/flask in T75 flasks. The numbers were counted using a Coulter Counter (Beckman Coulter) every 24 h. The ratios of CD133-positive cells were analyzed simultaneously by the above-mentioned method.

Statistical analysis

Experiments were performed three times each. The mean and standard deviations (SD) were calculated at each data point. Student's *t* test was used to analyze the significance of differences between groups. A probability (*P*) value of less than 0.05 was regarded as statistically significant. In

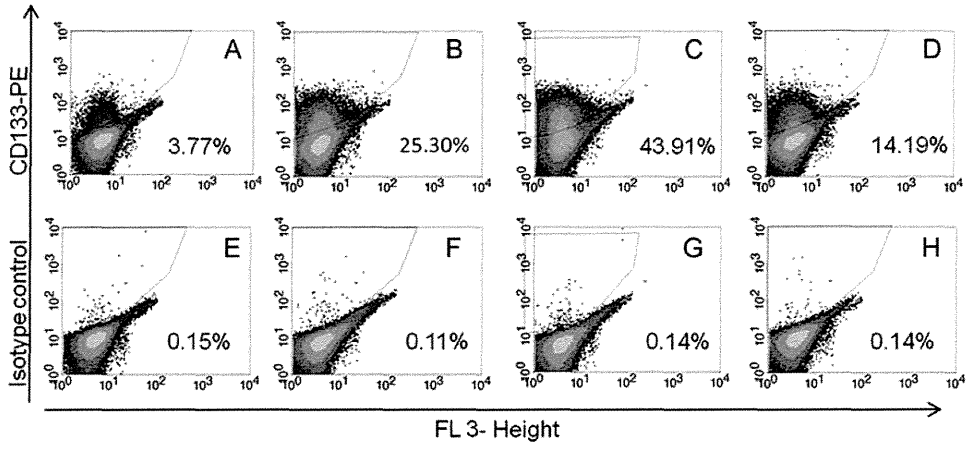

Fig. 1. Results of CD133 positivity analyses on the selected clones and the parental cells by flow cytometry. ONS-76 (**A**), ONS-F8 (**B**), ONS-B11 (**C**) and ONS-F11 (**D**) are results with CD133-PE antibody. ONS-76 (**E**), ONS-F8 (**F**), ONS-B11 (**G**) and ONS-F11 (**H**) are results with an isotype control antibody.

addition, linear regression analysis and confidence interval estimation were performed on the results of colony survival assay in which the 10% survival values (D_{10}) were obtained and surviving fraction at 2 Gy exposure (SF2) were calculated.

RESULTS

Isolation of surviving cells after irradiation

After γ-ray irradiation with 5 Gy, approximately 10500 ONS-76 cells in total number were seeded in 30 dishes. Consequently, 1440 colonies (13.7%) were formed after 2 weeks of incubation. From these colonies, 96 large colonies were selected by eye. Then, after another 5 Gy of γ-ray irradiation, 20 clones with high proliferative potency were selected and used in the further analyses (Supplemental Fig. 2 and Supplemental Fig. 4).

Screening of CD133 positivity

The results of CD133 positivity screening in the 20 clones are shown in Table 1. Parental ONS-76 contained 3.77% ± 0.09% CD133-positive cells (Fig. 1 and Table 1). The isolated clones showed a wide variation of CD133 positivities ranging from 0.06% to 43.91% (Table 1). Of these 20 clones, 12 clones showed a decreased CD133 positivity while 8 clones showed an increased CD133 positivity as compared with the parental ONS-76 cell line. Among 8 clones with increased CD133 level, 3 clones, namely ONS-F8, ONS-B11 and ONS-F11, showed significantly higher CD133-positive ratios of 25.30% ± 0.41%, 43.91% ± 2.08% and 14.19% ± 0.75%, respectively (Fig. 1 and Supplemental Fig. 3A). Thus, further analyses were focused on these three clones and the parental ONS-76 cell line.

Table 1. CD133 positive ratios in 20 isolated clones

Clones	CD133-positive ratio (%)	Clones	CD133-positive ratio (%)
ONS-76	3.77		
ONS-B11	43.91	ONS-H1	0.98
ONS-F8	25.30	ONS-B5	0.98
ONS-F11	14.19	ONS-D2	0.43
ONS-C7	7.21	ONS-H7	0.35
ONS-G8	6.34	ONS-C8	0.3
ONS-E10	6.29	ONS-B10	0.3
ONS-A6	5.85	ONS-E4	0.24
ONS-C1	5.35	ONS-B3	0.23
ONS-C10	3.46	ONS-H8	0.2
ONS-A10	1.06	ONS-C5	0.06

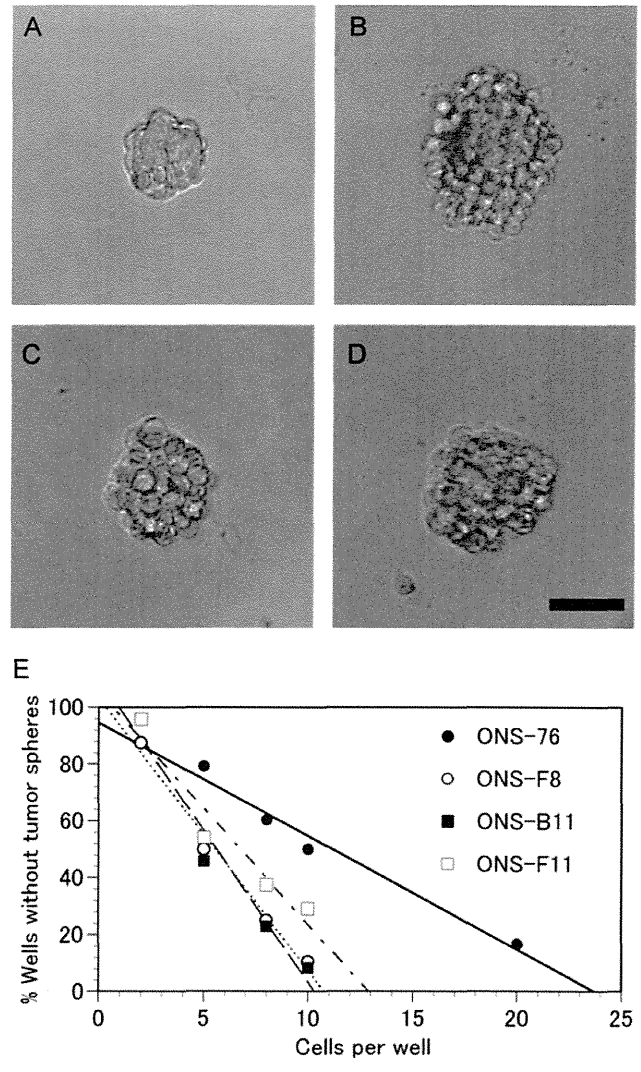

Fig. 2. Results of the tumor sphere formation assay. Photographs show tumor spheres from ONS-76 (**A**), ONS-F8 (**B**), ONS-B11 (**C**) and ONS-F11 (**D**). The black bar in the panel D indicates 300 μm in length. The tumor sphere formation abilities in ONS-76 (closed circles), ONS-F8 (open circles), ONS-B11 (closed squares) and ONS-F11 (open squares) were determined by the limiting dilution assay.

Tumor sphere formation ability

The results of tumor sphere formation assay of ONS-76, ONS-F8, ONS-B11 and ONS-F11 demonstrate that the calculated numbers of cells required to form at least one tumor sphere/well were 23.2 ± 0.9 in ONS-76, 10.8 ± 0.6 in ONS-F8, 10.3 ± 0.5 in ONS-B11 and 13.2 ± 2.3 in ONS-F11 (Fig. 2). Statistical analyses demonstrated that three isolated clones with high CD133 positivity have significantly higher tumor sphere formation ability as compared with the parental ONS-76 (Supplemental Fig. 3B).

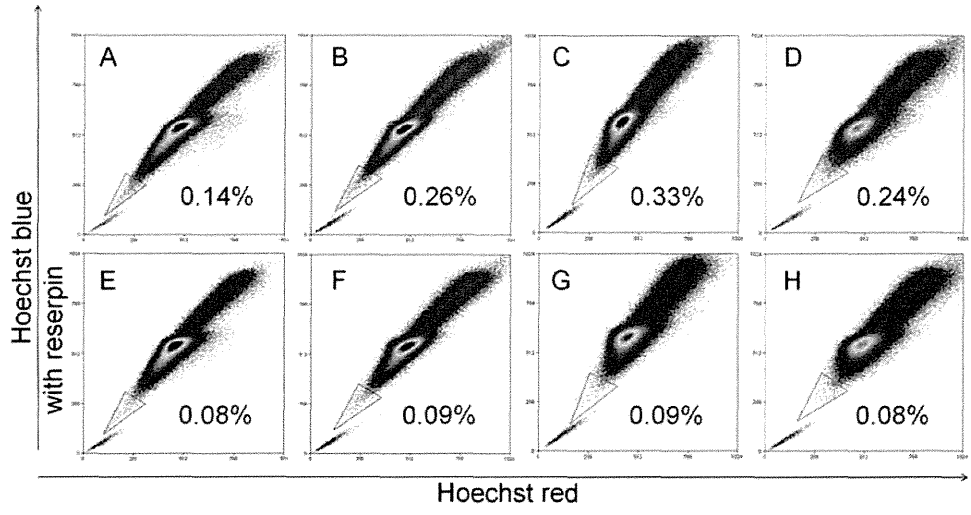

Fig. 3. Results of the side-population analysis. ONS-76 (**A**), ONS-F8 (**B**), ONS-B11 (**C**) and ONS-F11 (**D**) are results of flow cytometry with Hoechst 33342. ONS-76 (**E**), ONS-F8 (**F**), ONS-B11 (**G**) and ONS-F11 (**H**) are results after treatment with reserpine. Note that the side-population disappeared in E, F, G and H.

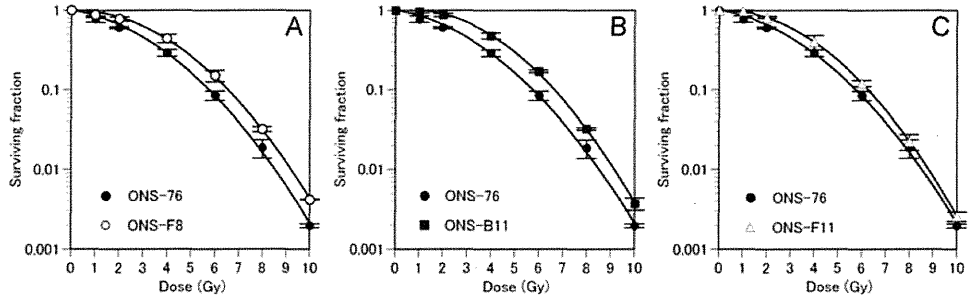

Fig. 4. Results of the clonogenic survival assay. (**A**) Survival curves of ONS-76 (closed circles) and ONS-F8 (open circles). (**B**) Survival curves of ONS-76 (closed circles) and ONS-B11 (closed circles). (**C**) Survival curves of ONS-76 (closed circles) and ONS-F11 (open triangles). The survival parameters were calculated by curve fitting with the LQ model. Error bars indicate standard deviation.

Percentage of side population cells

As shown in Fig. 3A–D, the percentages of the side population in ONS-76, ONS-F8, ONS-B11 and ONS-F11 were 0.14% ± 0.02%, 0.26% ± 0.02%, 0.33% ± 0.05% and 0.24% ± 0.02%, respectively. In each case, the side population was decreased significantly after treatment with reserpine (15 mg/ml) (Fig. 3E–H). Statistical analyses demonstrated that these three isolated clones had significantly higher side population cell fractions as compared with the parental ONS-76 (Supplemental Fig. 3C).

Clonogenic survival assay

To validate the radio-resistance of the three clones with high CD133 positivity, standard clonogenic survival assay was performed, and the results are shown in Fig. 4. The mean data points for each radiation treatment were curve-fitted by the LQ model. The error bars on the survival curves indicate the SD calculated from three independent experiments. The 10% survival values (D10) were 5.68 ± 0.13 Gy in ONS-76, 6.53 ± 0.15 Gy in ONS-F8, 6.64 ± 0.08 Gy in ONS-B11 and 6.26 ± 0.07 Gy in ONS-F11, and the survival fractions at 2 Gy (SF2) were 0.64% ± 0.03% in ONS-76, 0.82% ± 0.06% in ONS-F8, 0.90% ± 0.05% in ONS-B11 and 0.81% ± 0.07% in ONS-F11 (Table 2). Considering a 95% confidence interval (CI), these three isolated clones had significantly higher SF2 values as compared with the parental ONS-76 (Table 2).

Growth pattern and CD133-positive cell fraction

As shown in Fig. 5A, the numbers of cells of the three clones became greater than that of ONS-76 after 96 h of incubation although their growth patterns were similar. Also, it was shown that compared with CD133-negative cells, the percentage of CD133-positive cells in the three clones

Table 2. Calculated parameters of survival curves of ONS-76, ONS-F8, ONS-B11 and ONS-F11

	$\alpha(Gy^{-1}) \pm 95\%$ CI	$\beta(Gy^{-2}) \pm 95\%$ CI	R^2	SF2 ± 95%CI	D_{10} (Gy) ± 95% CI
ONS-76	0.13 ± 0.03	0.05 ± 0.003	0.99	0.64 ± 0.03	5.68 ± 0.13
ONS-F8	−0.01 ± 0.05	0.06 ± 0.005	0.99	0.82 ± 0.06	6.53 ± 0.14
ONS-B11	−0.07 ± 0.04	0.06 ± 0.005	0.99	0.90 ± 0.05	6.64 ± 0.08
ONS-F11	−0.016 ± 0.02	0.06 ± 0.004	0.99	0.81 ± 0.02	6.26 ± 0.07

Values of α and β with ±95% confidence interval (CI), and the coefficient of determination (R^2) were calculated by curve fitting with linear-quadratic (LQ) model. Values of SF2 indicate surviving fractions at dose of 2 Gy. D_{10} indicates dose corresponding to 10% surviving fraction. Values of 95% CI were calculated from three independent experiments.

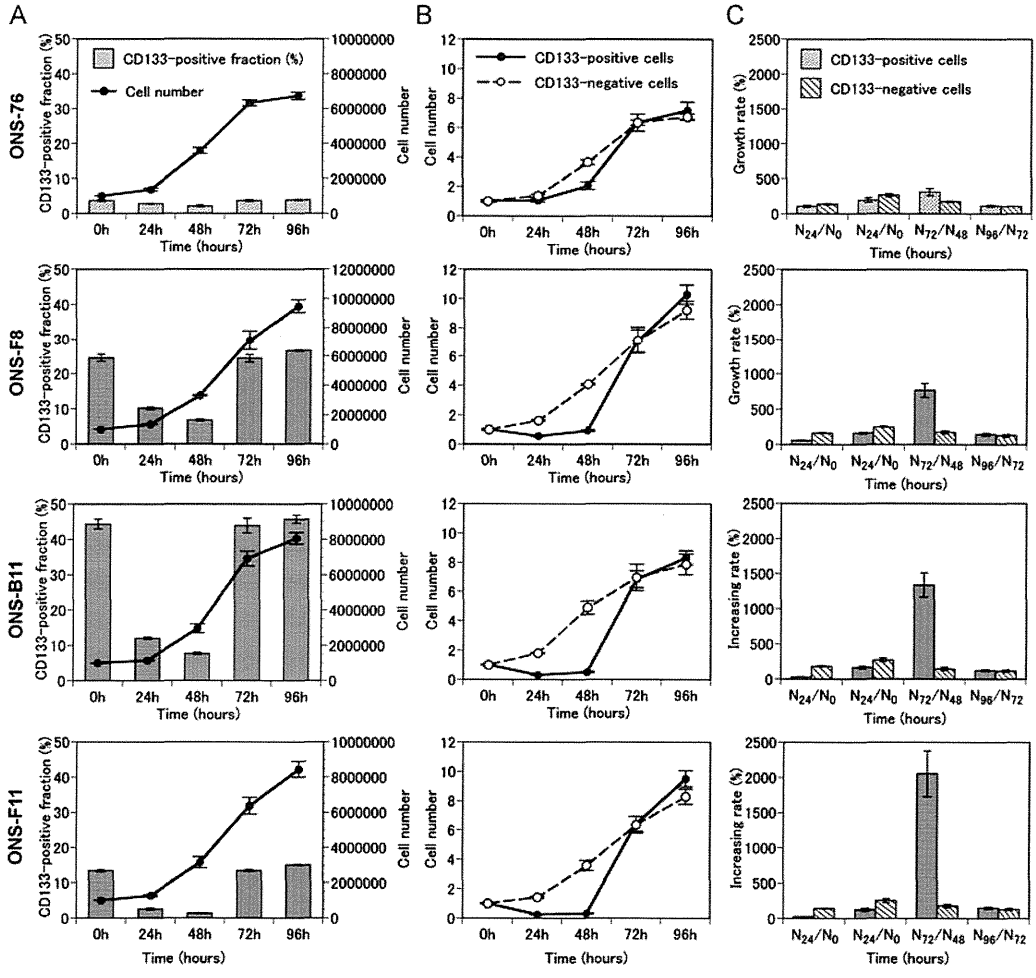

Fig. 5. Chronological changes of cell counts and CD133-positive fractions of the selected clones and the parental cells. (**A**) Cell counts (line graphs) and CD133-positive fractions (bar graphs) of ONS-76, ONS-F8, ONS-B11 and ONS-F11 were plotted against time. (**B**) Cell counts of CD133-positive cells (solid lines) and CD133-negative cells (dotted lines) of ONS-76, ONS-F8, ONS-B11 and ONS-F11 were plotted against time. Cell counts were normalized to 1 at 0 h. (**C**) Increase rates (%) of CD133-positive and CD133-negative cells of ONS-76, ONS-F8, ONS-B11 and ONS-F11at the time-points indicated. Error bars indicate standard deviation.

decreased from 0 to 48 h, and they increased rapidly from 48 to 72 h (Fig. 5B). The calculated maximum growth rates of CD133-positive cells were 310% ± 50% in ONS-76, 768% ± 96% in ONS-F8, 1338% ± 174% in ONS-B11 and 2053% ± 323% in ONS-F11 (Fig. 5C), which were significantly greater than the growth rates of 300% or less in CD133-negative cells in every cell line.

DISCUSSION

It has been postulated that a very small number of CSCs in tumor tissue survive radiotherapy and lead to tumor regeneration in various malignant tumors [21–22]. However, it has not been clarified whether radio-resistant subpopulations possess stemness in medulloblastoma cells. In this study, we aimed to confirm that medulloblastoma cells that survived γ-ray irradiation contain cells with stem cell-like characteristics *in vitro*. Thus, we recreated the process of tumor recurrence *in vitro* using γ-ray irradiation followed by resistant cell selection and characterizing their stemness.

Several attempts have been made to establish radio-resistant cells after exposure to single or fractionated irradiations, and their radio-resistant nature have been analyzed [23–24]. Wei *et al.* selected radio-resistant cells from human fibrosarcoma HT1080 through exposure to 2 Gy per day, 5 days per week for 7 months. Their radio-resistant cells had different G-banded karyotypes compared with parental cells [23]. Also, Tang *et al.* established two radio-resistant sublines of human hepatocellular carcinoma HepG2 cells by exposure to 2 Gy of γ-rays for 10 days or 10 Gy for 2 days. They found radio-resistant cells had a greater extent of potentially lethal damage repair (PLDR) and over-expression of Raf-1 [24]. More recently, Kuwahara *et al.* established radio-resistant cells from a human hepatocellular carcinoma cell line, HepG2, in which the cells were exposed once to 2 Gy of α-particles with boron neutron capture, followed by 0.5 Gy of X-rays at every 12-h interval for more than 6 years associated with 2 Gy of X-rays per day for 30 consecutive days [25–26]. These reported methods were most likely intended to induce mutations by irradiation over a certain period of time to produce stably radio-resistant cells. In contrast, our purpose here was to recreate tumor recurrence after radiotherapy and to evaluate stemness in surviving cells. Thus, we used a modified replica micro-well method to select clones after 5 Gy of γ-irradiation twice, based on our previous data that 5 Gy corresponded to approximately 20% survival in ONS-76 (Supplemental Fig. 1) [16]. Although a comparison between non-irradiated and irradiated clones may demonstrate the effect of irradiation more clearly, the chances of harvesting radio-resistant clones from non-irradiated cells without selection would be very low. Thus we evaluated stemness only on clones isolated by the method described above.

CD133 was originally found as a marker on neural stem-like cells [27–28]. In addition, CD133-positive cells were reported to have strong tumor-initiating and multilineage capacities in glioblastoma and medulloblastoma cells [12–13, 29]. Therefore, CD133 is recognized as one of the reliable markers of CSCs in these tumors. In this study, 20 selected radio-resistant clones expressed CD133 with a range from 0.06 to 44%, and three clones showed predominantly higher levels of CD133 positivity as compared with parental ONS-76 (Table 1 and Fig. 1). In addition, we confirmed that these three clones were stable in maintaining CD133 positivity even after 10 passages. Since it has been reported that CD133-negative cells do not spontaneously become CD133-positive after cell division, and irradiation itself does not induce CD133 expression in CD133-negative tumor cells, these three clones were most likely derived from cells that were originally CD133-positive [8]. Thus, our observation may indicate that these CD133-positive clones have strong self-renewal capacity to produce CD133-positive cells in a symmetric cell division pattern. As for the other 17 clones with CD133-positive ratios ranging from 0.06–7.21%, some of them may possess radio-resistant features due to other mechanisms that are not directly related to stemness, however, further characterization of these clones is out of the scope of the present study.

Other characteristics of CSCs in glioblastoma and medulloblastoma cells are sphere formation ability in optimum media [12, 30], and higher Hoechst 33342 effluxes side-population [19, 31–34]. We demonstrated that the three clones with high CD133-positive ratios also had significantly higher D_{10} and SF2 values, sphere formation ability and side-population fractions as compared with the parental ONS-76 (Figs 2, 3, 4, Supplemental Fig. 3 and Table 2). These results agree well with the reported data, which have demonstrated that side-population cells were expressing high levels of self-renewal-related genes such as notch and PTEN in brain tumor cells [14, 35]. However, although we performed double staining of CD133 and side-population in FACS analysis, we could not find a close correlation between these in the three isolated radio-resistant clones, indicating that they may contain different subtypes of cells with regard to stemness.

We observed that CD133-positive cells did not proliferate during the first 48 h of the incubation period, and they grew very rapidly thereafter (Fig. 5B). This may demonstrate that CD133-positive cells proliferated by symmetric cell divisions after remaining in the resting (G0) state for a latent period. Furthermore, maximum growth rates of CD133-positive cells in the three isolated clones were significantly higher than those to the parental ONS-76. From these observations, these three isolated clones possess not only self-renewal potency but also potentially high proliferative ability *in vitro* (Fig. 5C).

As for the mechanism of radio-resistance of CSCs, Bao *et al.* reported that the expression levels of checkpoint-related proteins such as ATM, Rad17, Chk1 and Chk2 were highly up-regulated in CSCs after irradiation, resulting in accumulation of cells in the cell cycle arrest in order to repair damaged DNA [8]. In addition, Diehn *et al.* demonstrated that CSCs had lower reactive oxygen species (ROS) levels with less DNA damages, which may suggest that CSCs had high radiation-induced free radical scavenge ability and had lower incidence of radical-induced DNA damages [36]. Also, it has been reported that the self-renewal-related notch pathway was closely associated with increase of the CD133-positive cell fractions and increase of radio-resistance in brain tumor cells [37]. Another self-renewal-related gene, BMI-1, was also reported to enhance radio-resistance in brain tumor cells [38]. These molecular analyses of the mechanism of self-renewal and radio-resistance may add further information to the characterization of the three clones isolated in this study.

To improve tumor control we must initially clarify resistance mechanisms. Elucidating the role of medulloblastoma stem cells in tumor response to radiation will enhance our understanding of the current status of radiotherapy against this pediatric brain tumor, and may help direct our research to achieving a more favorable outcome. Thus, future studies should be aimed at defining a specific method to disrupt the resistance mechanism of CSCs and improve overall tumor control. As mentioned above, the checkpoint kinases or self-renewal related genes may be possible molecular targets. At this point, however, it is mandatory to proceed with studies, not only to clarify the clinical applicability of these molecules, but also to find other novel molecules that are responsible for both stemness and radio-resistance.

In conclusion, we recreated the phenomenon of medulloblastoma recurrence after radiotherapy *in vitro*, and demonstrated that at least three clones among 20 survivors with high proliferative proficiency after γ-irradiation possess cancer stemness. These results should contribute to elucidating the mechanism of recurrence after radiotherapy in patients with medulloblastoma.

ACKNOWLEDGEMENTS

This work was partly supported by a Grant-in-Aid from the Ministry of Education, Culture, Sports, Science & Technology of Japan, and a research fund from the University of Tsukuba, Japan.

REFERENCES

1. Peris-Bonet R, Martinez-Garcia C, Lacour B *et al.* Childhood central nervous system tumours–incidence and survival in Europe (1978-1997): report from Automated Childhood Cancer Information System project. *Eur J Cancer* 2006;**42**:2064–80.
2. Oyharcabal-Bourden V, Kalifa C, Gentet JC *et al.* Standard-risk medulloblastoma treated by adjuvant chemotherapy followed by reduced-dose craniospinal radiation therapy: a French Society of Pediatric Oncology Study. *J Clin Oncol* 2005;**23**:4726–34.
3. Gajjar A, Chintagumpala M, Ashley D *et al.* Risk-adapted craniospinal radiotherapy followed by high-dose chemotherapy and stem-cell rescue in children with newly diagnosed medulloblastoma (St Jude Medulloblastoma-96): long-term results from a prospective, multicentre trial. *Lancet Oncol* 2006;**7**:813–20.
4. Massimino M, Giangaspero F, Garre ML *et al.* Childhood medulloblastoma. *Crit Rev Oncol Hematol* 2011;**79**:65–83.
5. Habrand JL, De Crevoisier R. Radiation therapy in the management of childhood brain tumors. *Childs Nerv Syst* 2001;**17**:121–33.
6. Cervoni L, Cantore G. Medulloblastoma in pediatric age: a single-institution review of prognostic factors. *Childs Nerv Syst* 1995;**11**:80–4; discussion 85.
7. Dennis M, Spiegler BJ, Hetherington CR *et al.* Neuropsychological sequelae of the treatment of children with medulloblastoma. *J Neurooncol* 1996;**29**:91–101.
8. Bao S, Wu Q, McLendon RE *et al.* Glioma stem cells promote radioresistance by preferential activation of the DNA damage response. *Nature* 2006;**444**:756–60.
9. Chiou SH, Kao CL, Chen YW *et al.* Identification of CD133-positive radioresistant cells in atypical teratoid/rhabdoid tumor. *PLoS One* 2008;**3**:e2090.
10. Blazek ER, Foutch JL, Maki G. Daoy medulloblastoma cells that express CD133 are radioresistant relative to CD133- cells, and the CD133+ sector is enlarged by hypoxia. *Int J Radiat Oncol Biol Phys* 2007;**67**:1–5.
11. Vlashi E, Lagadec C, Vergnes L *et al.* Metabolic state of glioma stem cells and nontumorigenic cells. *Proc Natl Acad Sci USA* 2011;**108**:16062–67.
12. Singh SK, Clarke ID, Terasaki M *et al.* Identification of a cancer stem cell in human brain tumors. *Cancer Res* 2003;**63**:5821–8.
13. Singh SK, Hawkins C, Clarke ID *et al.* Identification of human brain tumour initiating cells. *Nature* 2004;**432**:396–401.
14. Fan X, Matsui W, Khaki L *et al.* Notch pathway inhibition depletes stem-like cells and blocks engraftment in embryonal brain tumors. *Cancer Res* 2006;**66**:7445–52.
15. Tamura K, Shimizu K, Yamada M *et al.* Expression of major histocompatibility complex on human medulloblastoma cells with neuronal differentiation. *Cancer Res* 1989;**49**:5380–4.
16. Gerelchuluun A, Hong Z, Sun L *et al.* Induction of in situ DNA double-strand breaks and apoptosis by 200 MeV protons and 10 MV X-rays in human tumour cell lines. *Int J Radiat Biol* 2011;**87**:57–70.
17. Kunkele A, De Preter K, Heukamp L *et al.* Pharmacological activation of the pp53 pathway by nutlin-3 exerts anti-tumoral effects in medulloblastomas. *Neuro Oncol* 2012;**14**:859–69.
18. Tsuboi K, Tsuchida Y, Endo K *et al.* Isolation of radiosensitive and radioresistant mutants from a medulloblastoma cell line. *Brain Tumor Pathol* 1997;**14**:19–25.

19. Ho MM, Ng AV, Lam S *et al.* Side population in human lung cancer cell lines and tumors is enriched with stem-like cancer cells. *Cancer Res* 2007;**67**:4827–33.
20. Franken NA, Rodermond HM, Stap J *et al.* Clonogenic assay of cells in vitro. *Nat Protoc* 2006;**1**:2315–19.
21. Rich JN. Cancer stem cells in radiation resistance. *Cancer Res* 2007;**67**:8980–4.
22. Visvader JE, Lindeman GJ. Cancer stem cells in solid tumours: accumulating evidence and unresolved questions. *Nat Rev Cancer* 2008;**8**:755–68.
23. Wei K, Kodym R, Jin C. Radioresistant cell strain of human fibrosarcoma cells obtained after long-term exposure to x-rays. *Radiat Environ Biophys* 1998;**37**:133–7.
24. Tang WY, Chau SP, Tsang WP *et al.* The role of Raf-1 in radiation resistance of human hepatocellular carcinoma Hep G2 cells. *Oncol Rep* 2004;**12**:1349–54.
25. Kuwahara Y, Li L, Baba T *et al.* Clinically relevant radioresistant cells efficiently repair DNA double-strand breaks induced by X-rays. *Cancer Sci* 2009;**100**:747–52.
26. Kuwahara Y, Mori M, Oikawa T *et al.* The modified high-density survival assay is the useful tool to predict the effectiveness of fractionated radiation exposure. *J Radiat Res* 2010;**51**:297–302.
27. Coskun V, Wu H, Blanchi B *et al.* CD133+ neural stem cells in the ependyma of mammalian postnatal forebrain. *Proc Natl Acad Sci USA* 2008;**105**:1026–31.
28. Kania G, Corbeil D, Fuchs J *et al.* Somatic stem cell marker prominin-1/CD133 is expressed in embryonic stem cell-derived progenitors. *Stem Cells* 2005;**23**:791–804.
29. Qiang L, Yang Y, Ma YJ *et al.* Isolation and characterization of cancer stem like cells in human glioblastoma cell lines. *Cancer Lett* 2009;**279**:13–21.
30. Ghods AJ, Irvin D, Liu G *et al.* Spheres isolated from 9L gliosarcoma rat cell line possess chemoresistant and aggressive cancer stem-like cells. *Stem Cells* 2007;**25**: 1645–53.
31. Fukaya R, Ohta S, Yamaguchi M *et al.* Isolation of cancer stem-like cells from a side population of a human glioblastoma cell line, SK-MG-1. *Cancer Lett* 2010;**291**:150–7.
32. Kondo T, Setoguchi T, Taga T. Persistence of a small subpopulation of cancer stem-like cells in the C6 glioma cell line. *Proc Natl Acad Sci USA* 2004;**101**:781–6.
33. Chiba T, Kita K, Zheng YW *et al.* Side population purified from hepatocellular carcinoma cells harbors cancer stem cell-like properties. *Hepatology* 2006;**44**:240–51.
34. Patrawala L, Calhoun T, Schneider-Broussard R *et al.* Side population is enriched in tumorigenic, stem-like cancer cells, whereas ABCG2+ and ABCG2- cancer cells are similarly tumorigenic. *Cancer Res* 2005;**65**:6207–19.
35. Bleau AM, Hambardzumyan D, Ozawa T *et al.* PTEN/PI3K/Akt pathway regulates the side population phenotype and ABCG2 activity in glioma tumor stem-like cells. *Cell Stem Cell* 2009;**4**:226–35.
36. Diehn M, Cho RW, Lobo NA *et al.* Association of reactive oxygen species levels and radioresistance in cancer stem cells. *Nature* 2009;**458**:780–3.
37. Wang J, Wakeman TP, Lathia JD *et al.* Notch promotes radioresistance of glioma stem cells. *Stem Cells* 2010;**28**: 17–28.
38. Facchino S, Abdouh M, Chatoo W *et al.* BMI1 confers radioresistance to normal and cancerous neural stem cells through recruitment of the DNA damage response machinery. *J Neurosci* 2010;**30**:10096–111.

Clinical Neurophysiology 123 (2012) 1496–1501

Contents lists available at SciVerse ScienceDirect

Clinical Neurophysiology

journal homepage: www.elsevier.com/locate/clinph

sLORETA-qm for interictal MEG epileptic spike analysis: Comparison of location and quantity with equivalent dipole estimation

T. Uda [a,*], N. Tsuyuguchi [a], E. Okumura [b], S. Sakamoto [c], M. Morino [d], T. Nagata [a], H. Ikeda [a], N. Kunihiro [a], T. Takami [a], K. Ohata [a]

[a] Department of Neurosurgery, Osaka City University Graduate School of Medicine, Osaka, Japan
[b] MEG Gr. Bio and Analytical Center, Yokogawa Electric Corporation, Kanazawa, Japan
[c] Department of Radiology, Osaka City University Graduate School of Medicine, Osaka, Japan
[d] Department of Neurosurgery, Tokyo Metropolitan Neurological Hospital, Tokyo, Japan

ARTICLE INFO

Article history:
Accepted 14 December 2011
Available online 31 January 2012

Keywords:
sLORETA
Equivalent current dipole
Epilepsy
Interictal spike
MEG

HIGHLIGHTS

- Magnetic source location and quantity were compared between quantitative modification of a standardised low-resolution brain electromagnetic tomography (sLORETA-qm) and equivalent current dipole (ECD) for analysis of the interictal epileptic spike.
- sLORETA-qm closely correlated with ECD concerning point source location and quantity.
- sLORETA-qm is a reliable quantifiable method without arbitrariness that can be used for analysis of the interictal epileptic spike.

ABSTRACT

Objective: To determine whether quantitative modification of a standardised low-resolution brain electromagnetic tomography (sLORETA-qm) could be used as a reliable tool for quantitative analysis of magnetoencephalography (MEG) for analysis of the interictal epileptic spike. To verify the performance of sLORETA-qm, magnetic source location and quantity were compared with the equivalent current dipole (ECD) method.
Methods: A total of 50 sources from 10 patients with epilepsy were obtained. Analyses were performed after the MEG data were 3–70 Hz band-pass filtered. Time points for analysis were selected referring to waveform patterns and the isofield contour map. With the same spherical model, source estimation was conducted with two methods of analysis: ECD and sLORETA-qm. Distance from the centre of the spherical model and intensities were compared between the methods.
Results: There were no significant differences between the methods in the distance from the spherical model (paired t-test, $p = 0.8761$). Source intensities between the methods were strongly correlated (Spearman's Rho = 0.9803, $p < 0.001$).
Conclusions: sLORETA-qm was closely correlated with ECD concerning point source location and quantity in analysis of the interictal epileptic spike.
Significance: sLORETA-qm is a reliable quantifiable method without arbitrariness for analysis of the interictal epileptic spike.

1. Introduction

An epileptogenic zone is defined as the zone of actual seizure onset that needs to be removed in order to achieve seizure freedom (Penfield and Jasper, 1954). In preoperative evaluation of epilepsy, it is preferable to record the ictal epileptiform discharge in electroencephalography (EEG) or magnetoencephalography (MEG) in order to detect the epileptogenic zone. Chances to record a seizure from a patient are rather low because of limited recording time; so it is important to detect the irritative zone that demonstrates the interictal focal epileptiform discharge due to paroxysmal neuronal activity.

Paroxysmal interictal epileptiform discharge generates a strong magnetic flux compared to normal spontaneous magnetic activity of the brain. For analysis of interictal epileptiform discharge, the equivalent current dipole (ECD) estimation method is commonly

* Corresponding author. Address: Department of Neurosurgery, Osaka City University Graduate School of Medicine, 1-4-3 Asahi-machi, Abeno-ku, Osaka 545-8585, Japan. Tel.: +81 6 6645 3846; fax: +81 6 6647 8065.
E-mail address: uda@med.osaka-cu.ac.jp (T. Uda).

1388-2457/$36.00 © 2011 International Federation of Clinical Neurophysiology. Published by Elsevier Ireland Ltd. All rights reserved.
doi:10.1016/j.clinph.2011.12.008

used, especially for clinical evaluation. In this method, a single source at a single time point is estimated from the surface magnetic field distribution, and the location, intensity and orientation of the source are obtained.

Although the ECD estimation method is a simple and useful model for solving the electromagnetic inverse problem, it has two problems concerning objective assessment of the electromagnetic activity: restricted numbers of current sources and arbitrary sensor selection.

Spatial filtering techniques are alternative approaches to these problems. Standardised low-resolution brain electro-magnetic tomography (sLORETA) is a non-adaptive spatial filtering technique that has been reported previously (Pascual-Marqui, 2002), and has no localisation bias under ideal conditions (Greenblatt et al., 2005; Sekihara et al., 2005). This technique can be used to determine the localisation of magnetic activities, even for multiple sources (Wagner et al., 2004), unless the sources are located in close proximity to each other. Furthermore, source reconstruction by sLORETA can be performed without sensor selection, and therefore arbitrariness of sensor selection can be avoided. Moreover, sLORETA can also provide pseudo-statistic values, which can be used as estimates of the degree of activity. These properties are highly advantageous for quantitative analysis of MEG in a clinical setting.

To establish sLORETA as a quantifiable method, sLORETA was modified and named sLORETA-qm (Terakawa et al., 2008). The use of sLORETA-qm with the somatosensory evoked field (SEF) has been reported previously (Terakawa et al., 2008). According to that report, the ECD moment and sLORETA-qm intensity were highly correlated with the SEF. Moreover, sLORETA-qm was applied to assess spontaneous neuromagnetic slow wave activity (Sakamoto et al., 2010). In that report, neuromagnetic slow wave activity was demonstrated to be distributed in the area of ischaemic brain lesions, and the activity intensity decreased after surgery performed to improve cerebral blood flow. It has been reported that sLORETA-qm may offer a novel, non-invasive method for identification and quantification of cerebral ischaemia. However, it remains unclear whether this modification of sLORETA can be applied to the interictal epileptic spike discharge, in other words, spontaneous paroxysmal magnetic activity without averaging.

The present study was performed to determine whether sLORETA-qm spatial filtering could be used as a reliable tool for quantitative analysis of the MEG interictal epileptic spike discharge. To verify the performance of sLORETA-qm, magnetic source location and quantity were compared with the conventional ECD method.

2. Methods

2.1. Patients

All 10 patients (six men and four women, ranging in age from 20 to 55 years) with medically refractory partial epilepsy and demonstrating interictal epileptic spike discharges in EEG and MEG, who were admitted to Department of Neurosurgery, Osaka City University Hospital between May 2008 and March 2010 and met the following inclusion criteria, were retrospectively included in the study. Patient characteristics are shown in Table 1. They all had epilepsy surgery at Osaka City University Hospital after MEG, and were followed up for at least 1 year after surgery. All subjects gave their informed consent, and the study was approved by the Ethics Committee of Osaka City University Hospital.

2.2. MEG measurement protocol

MEG was performed in a magnetically shielded room at Osaka City University Hospital using a 160-sensor helmet-type MEG system (Yokogawa Electric Corporation, Tokyo, Japan) with a magnetic field resolution of 4 fT/Hz1/2 in the white noise region. Sensing and reference coils in this system are both 15.5 mm in diameter, with a 50-mm baseline and 23 mm of separation between each pair of sensing coils. The subjects were positioned in the supine position with their eyes closed, with use of a horizontal-type dewar. MEG data were recorded through a 1- to 200-Hz band-pass filter with a sampling rate of 1000 Hz. The MEG acquisition time was 20 min. In addition, 19 electroencephalography (EEG) leads were recorded simultaneously, according to the international 10–20 system.

Table 1
Patient characteristics and spike origin.

Case	Age (years)	Gender	Spike origin
1	23	M	bil T
2	32	M	Lt T
3	55	M	Lt F
4	38	M	Rt F
5	28	F	Lt F
6	24	F	Rt T, Rt F
7	20	F	Rt F, Rt T, Lt O
8	30	M	bil T
9	47	F	bil O, Rt T
10	34	M	Rt T

M, male; F, female; bil, bilateral; Rt, right; Lt, left;T, temporal; F, frontal; O, occipital.

2.3. Data analysis

To reduce noise caused by the surrounding environment, data from the reference magnetometers, which were located outside of the dewar and picked up only environmental noise, were subtracted from the obtained MEG data.

As an epileptic spike discharge is defined as having a duration of 20 to less than 70 ms (IFSECN, 1974), the MEG data were band-pass filtered to cover this duration between 3 and 70 Hz (Papanicolaou, 2009). Time points for analysis were selected referring to the waveform patterns of MEG and EEG, and the isofield contour map of MEG. The following two methods of analysis, ECD and sLORETA-qm, were conducted using the same spherical model. Three-dimensional coordinates, distance from the centre of the spherical model and intensities were obtained by the two analytical methods and recorded for analysis.

2.3.1. ECD

Twenty sensors around the centre of the maximum extremum (the point at which the magnetic flux exits) and the minimum extremum (where the flux re-enters the head) on the isofield contour map were selected, and a magnetic source was estimated at a selected time point with the single dipole estimation method (Cuffin, 1985; Scherg and Von Cramon, 1986). Dipoles estimated with over 90% goodness of fit (GOF) were adopted as successful source estimations.

2.3.2. sLORETA-qm

MEG data from all sensors (160 sensors) were used for analysis. The brain area in the spherical model was divided into approximately 13,000 voxels with a spacing of $5 \times 5 \times 5$ mm^3. The actual voxel count depended on the head size of each subject, and ranged from 11,668 to 18,796. Voxels in areas with no effect of brain activities in the cerebral cortex (such as the cerebellum, brain stem, and in the vicinity of the eyes) were excluded. Voxels within 25% of the radius of the spherical model were also excluded. These operations were performed automatically by referring to the spherical model of each subject. In Fig. 1, adopted voxels are shown in pink. Previous reports have described how to obtain quantitative multiple

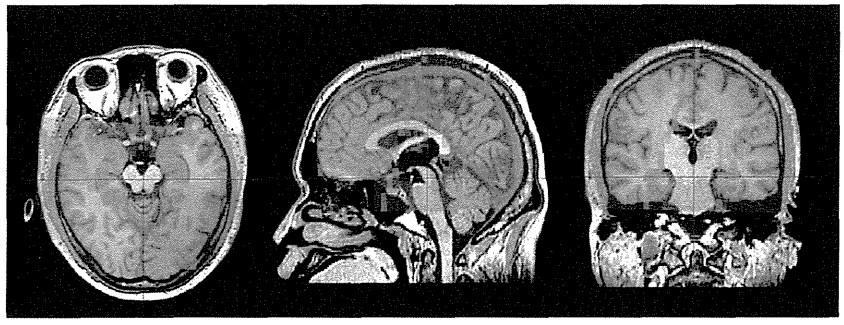

Fig. 1. Brain area in the spherical model is divided into voxels with a volume of $5 \times 5 \times 5$ mm^3. Adopted voxels are shown in pink. Voxels in areas with no effect from brain activities in the cerebral cortex (such as cerebellum, brain stem, and the vicinity of the eyes) are excluded. Voxels within 25% of the radius of the spherical model are also excluded.

source estimation using sLORETA-qm (Sakamoto et al., 2010; Terakawa et al., 2008). In short, the source reconstruction was performed by sLORETA at each time point as a first step (Pascual-Marqui, 2002). Subsequently, a voxel with a spatially maximum or local maximum intensity at each time point was chosen as a peak source. Finally, on the voxel chosen as the peak source, the quantified source intensity was estimated by correcting the lead-field component. The centre of the voxel was used as the three-dimensional coordinate. Source estimation with sLORETA-qm was computed with custom software developed using MATLAB version 7.7 (MathWorks Inc., Natick, MA, USA).

2.4. Evaluation

If the distances between the sources in the two analytical methods [(a) in Fig. 2] were less than 5 mm (same as the voxel diameter), these sources were considered concordant. In order to compare the location of the source between the two methods of analysis, distances from the centre of the spherical model [(b) and (c) in Fig. 2] were measured for each spike. A paired sample t-test was used to identify differences in distance from the spherical centre between the two methods after confirming the data were normally distributed (assessed by the Shapiro–Wilk test).

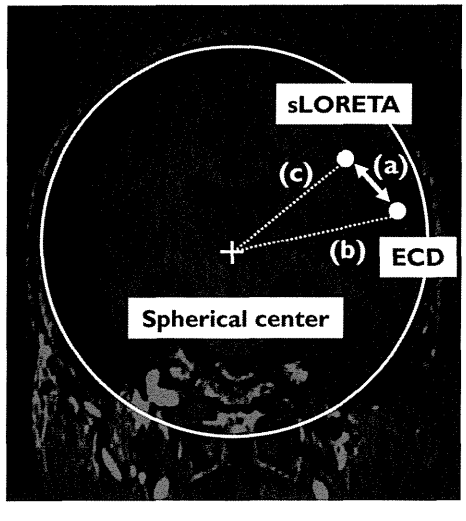

Fig. 2. Summary of analysed parameters: (a) distances between sources estimated by the equivalent current dipole (ECD) and by quantitative modification of standardised low-resolution brain electromagnetic tomography (sLORETA-qm), (b) distance from the centre of the spherical model to the source estimated by ECD, and (c) distance from the centre of the spherical model to the source estimated by sLORETA-qm. Circle indicates the radius of the spherical model.

To study the relationships of the intensities between the two methods, a non-parametric correlation coefficient (Spearman's Rho) was used because the intensities of the two methods were not normally distributed (Shapiro–Wilk test). Probability values less than 0.05 were considered significant in all statistical analyses. The software JMP 9.0 for Windows (SAS Institute Inc., Cary, NC, USA) was used for statistical evaluation.

3. Results

A total of 50 concordant sources (five interictal epileptic spikes for each patient) were used for analysis. The distance between the corresponding two sources [(a) in Fig. 2] and source intensities from the two methods are summarised in Table 2.

3.1. Distance from the centre of the spherical model to the estimated sources

The distances from the centre of the spherical model to the estimated sources were 57.95 ± 12.96 mm (mean ± SD) in ECD and 57.99 ± 12.81 mm (mean ± SD) in sLORETA-qm [(b) and (c) in Fig. 2, respectively]. There were no significant differences between the two distances (paired sample t-test, $p = 0.8761$).

3.2. Source intensities

As a result of correlation analysis, a close correlation was found between the two source intensities (Spearman's correlation coefficient, Rho = 0.9619, $p < 0.001$) (Fig. 3).

3.3. Representative case

3.3.1. Case 1_23-year-old man

The overlaid waveform of all 160 sensors is shown in Fig. 4A. High-amplitude magnetic flux was recorded around the time point of 1597 ms. In Fig. 4B, the isofield contour map at the time point of 1597 ms was depicted. The maximum extremum and the minimum extremum were recognised in the left temporal area. In ECD, 20 sensors around the centre of the maximum extremum and minimum extremum were selected (blue dots and sensor numbers in Fig. 4B). Waveforms of the 20 selected sensors are shown in Fig. 4C. Magnetic sources were estimated with the single dipole estimation method. The source was estimated with 94.56% GOF and the intensity of the source was 137.77 nAm. The distance from the spherical centre was 55.53 mm. In sLORETA-qm, all 160 sensors were used for source estimation. A total of three sources could be estimated, and the source intensities were 164.05, 66.19, and 39.80 nAm (Fig. 5). The peak voxel was located in left temporal lobe [(a) in Fig. 5] and the distance from the spherical

Table 2
Characteristics of estimated sources determined by equivalent current dipole (ECD) and quantitative modification of standardised low-resolution brain electromagnetic tomography (sLORETA-qm).

	Distance between the two sources* [median (range)] (mm)	Intensity range (nAm)
ECD	3.53 (1.28–4.98)	72.35–767.62
sLORETA-qm		62.89–716.54

* (a) in Fig. 1.

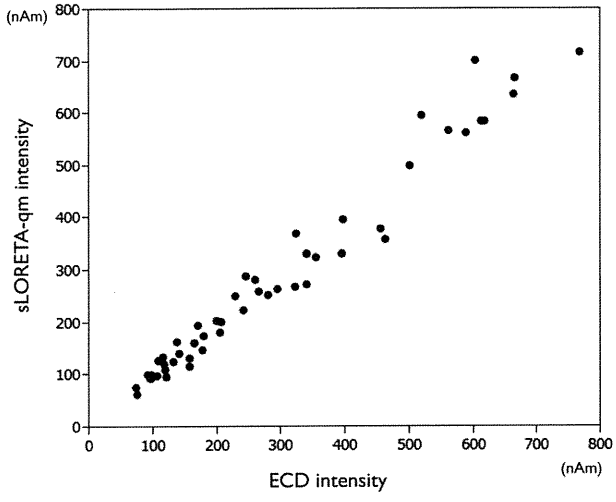

Fig. 3. The correlation between intensities from equivalent current dipole (ECD) and quantitative modification of standardised low-resolution brain electromagnetic tomography (sLORETA-qm) is depicted as a scatter plot. A close correlation is found between the two values (Spearman's correlation coefficient, Rho = 0.9803, $p < 0.001$).

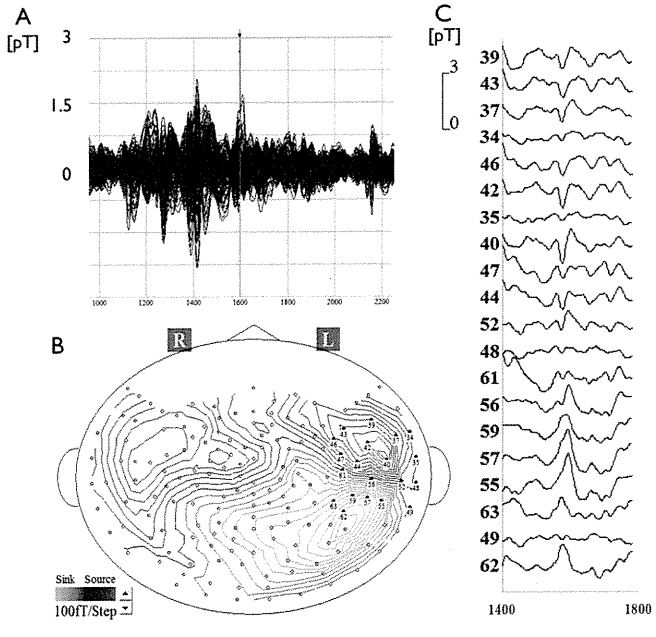

Fig. 4. (A) An overlaid waveform of all 160 sensors between 1000 ms and 2200 ms is demonstrated. High amplitude magnetic flux was recorded around 1597 ms. (B) Isofield contour map at the time point of 1597 ms is depicted. The maximum extremum (red contour) and minimum extremum (green contour) are recognised on the left temporal area. Blue dots indicate the 20 selected sensors used for analysis of the equivalent current dipole (ECD). (C)Waveforms of 20 selected sensors are shown.

centre was 55.94 mm. Estimated sources from the two analytical methods were superimposed on the patient's brain (Fig. 6). In this figure, the estimated source and orientation by ECD are depicted with a blue square and tail, respectively. The estimated peak source by sLORETA-qm is depicted as pink and white ellipse. The distance between the two sources is 4.33 mm.

4. Discussion

The present study evaluated the relationship between the sLORETA-qm and ECD concerning source location and quantity of the interictal epileptic discharge. In the analysed range of intensities (approximately 70–700 nAm), ECD dipole moments and sLORETA-qm intensities were closely correlated. There was no significant tendency concerning the distance from the centre of the spherical model between the two methods. To our knowledge, there have been no previous reports that have compared sLORETA-qm and ECD point source localisation and quantification during analysis of the interictal spike discharge in MEG.

ECD is a conventional and widely used approach, especially for studying the interictal epileptic spike discharge (Assaf et al., 2004; Iwasaki et al., 2002; Sakamoto et al., 2003). However, there are several problems concerning application of the ECD model to interictal epileptic spike discharge. The main problem is derived from the fact that all sensors cannot be taken into account when estimating the ECD source. In addition, the number of sources must be assumed by the isofield contour map before fitting the dipole model. Sensor location and the number of sensors selected depend on the examiner's experience and preference. Subjective and objective assessments of the irritative zone from the patient's ictal symptom may also affect sensor selection. Consequently, source location and quantity can be arbitrarily changed by each examiner, especially in the case of multiple sources. Another problem is that the sources are estimated as a maximum intensity spot, not a distributed area as in ECD. Considering that epileptic activities are often associated with multiple sources, and they are usually distributed in some areas of the brain, the use of spatial filtering in analysis of epileptic activities may be appropriate.

One of many kinds of spatial filtering techniques, sLORETA was adopted in the present report. sLORETA is one of the non-adaptive beamformer methods. Although non-adaptive beamformer methods generally have low resolution compared with adaptive beamformer methods (Sekihara and Nagarajan, 2008), there are two advantages with this type of technique for analysing the interictal spike. First, non-adaptive beamformer methods can reconstruct the source image from a single time point, but beamformer methods invariably need time course information for weight calculation in each voxel. Considering that the epileptic spike is instant electrical activity in the brain, non-adaptive beamformer methods may be more appropriate spatial filtering for interictal spike activity. Second, sLORETA can provide a quantitative source power with the unit of current intensity (nAm); otherwise, beamformer methods only offer a relative statistical value. This is advantageous when comparing the source power with ECD.

In spatial filtering techniques, including sLORETA-qm, signals from deeply located voxels are usually enhanced compared to signals in superficially located voxels. Therefore, in order to assess the tendency of source locations, the distance from the spherical centre was compared between these two methods. As a result, there were no significant differences between the two distances (paired sample t-test, $p = 0.8761$). To prevent false negative (beta) errors, a *post hoc* power analysis (using alpha = 5%) was performed on the data in order to calculate the required sample size for detecting a relevant difference. A relevant difference was defined as more than 2.5 mm (half of the voxel size) distance between

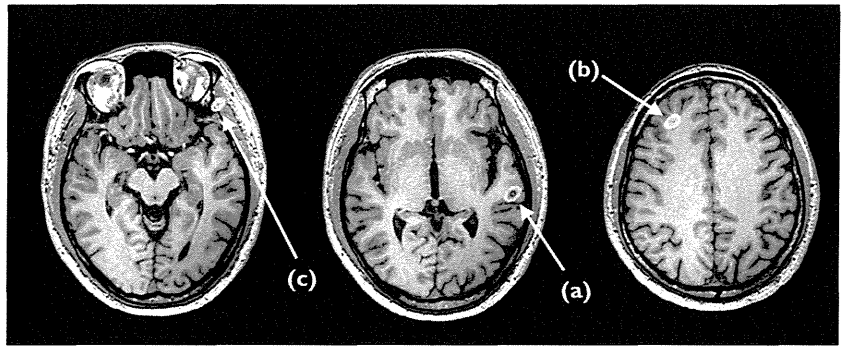

Fig. 5. A total of three sources estimated by quantitative modification of standardised low-resolution brain electromagnetic tomography (sLORETA-qm) are shown in pink and white ellipses. The source intensities are 164.05, 66.19 and 39.80 nAm for (a), (b) and (c), respectively. The peak voxel is located in the left temporal lobe (a), and the distance from the spherical centre is 55.94 mm.

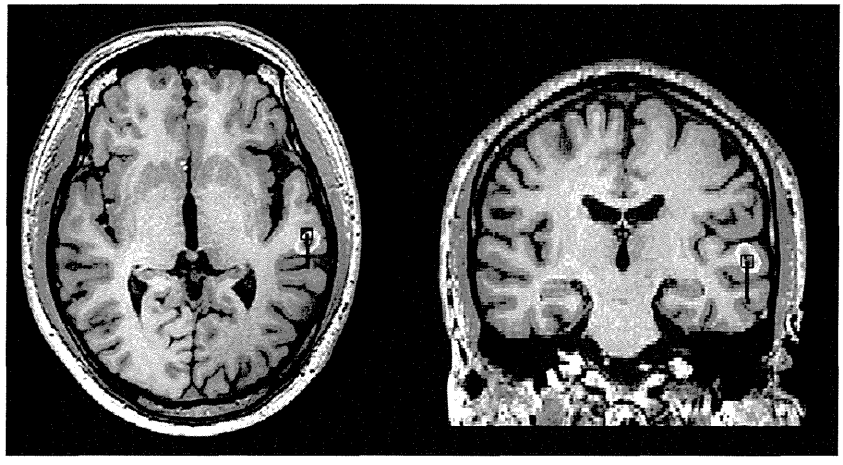

Fig. 6. Sources estimated by two analytical methods superimposed on the patient's brain. Blue square and tail indicate the estimated source and orientation by ECD, respectively. Pink and white ellipses indicate the estimated source by standardised low-resolution brain electromagnetic tomography (sLORETA-qm). The distance between the two sources is 4.33 mm.

the two methods. This analysis showed that the present study had sufficient power to detect a relevant difference at the 99.9% level. Consequently, the sample size ($n = 50$) in the present study was considered to be large enough for detection of a relevant difference between groups.

In a previous report, SEF intensities determined by ECD and sLORETA-qm were significantly correlated in the range of approximately 10–70 nAm (Terakawa et al., 2008). The analysed range of the source intensities in the present study was approximately 70–700 nAm, and close correlation between the intensities determined by the two methods was demonstrated with the Spearman's correlation coefficient. Thus, intensities obtained by sLORETA-qm may be reliable and quantitative over a wide range of intensities of paroxysmal interictal epileptic discharge.

A disadvantage of sLORETA-qm is that sources without clinical significance are often estimated. In the representative case in the present study, a total of three sources were estimated at the selected time point. The peak source amongst the estimated sources by sLORETA-qm corresponded to the source by ECD, and it could be distinguished as a clinically significant source. However, especially in the more complex isofield contour patterns, such as spatially close or synchronised multiple sources, it may be difficult to distinguish clinically significant sources among the estimated sources. This is one of the limitations of the spatial filtering technique. If the number of estimated sources is limited to one in the sLORETA-qm analysing process, only one source will be obtained and that source will be corresponded with the source by ECD. However, limiting the number of sources in analysis is somewhat arbitrary. Therefore, the number of estimated sources was not limited in the present study.

sLORETA-qm has a methodological limitation. The analytical results of sLORETA-qm depend on voxel size. The estimated localisation of the MEG sources can be restricted by its lattice, which can result in some localisation error. In the present study, the voxel diameter was 5 mm and the possible maximum localisation error derived from the voxel setting was 4.33 mm (the distance between the centre and apex of a voxel). This was because concordant sources were defined as a distance between the two sources of less than 5 mm, and only the concordant sources were adopted for the analysis.

In the present study, in order to verify the performance of sLORETA-qm, time points with typical maximum extremum and minimum extremum depicted on the isofield contour map were selected for analysis. For future studies, more complex isofield contour patterns should be analysed with sLORETA-qm. Although multiple sources are often difficult to analyse using only ECD, added use of sLORETA-qm may be helpful for evaluation of these complex epileptic spike discharges.

5. Conclusions

sLORETA-qm showed a close correlation with ECD in point source location and quantity for analysis of the interictal epileptic

spike, and is a reliable quantifiable method without arbitrariness for analysis of the interictal epileptic spike.

Acknowledgement

None of the authors has any conflicts of interest to disclose.

References

Assaf BA, Karkar KM, Laxer KD, Garcia PA, Austin EJ, Barbaro NM, et al. Magnetoencephalography source localization and surgical outcome in temporal lobe epilepsy. Clin Neurophysiol 2004;115:2066–76.

Cuffin BN. A comparison of moving dipole inverse solutions using EEG's and MEG's. IEEE Trans Biomed Eng 1985;32:905–10.

Greenblatt RE, Ossadtchi A, Pflieger ME. Local linear estimators for the bioelectromagnetic inverse problem. IEEE Trans Biomed Eng 2005;53:3403–12.

IFSECN. A glossary of terms most commonly used by clinical electroencephalographers. Electroencephalogr Clin Neurophysiol 1974;37:538–48.

Iwasaki M, Nakasato N, Shamoto H, Nagamatsu K, Kanno A, Hatanaka K, et al. Surgical implications of neuromagnetic spike localization in temporal lobe epilepsy. Epilepsia 2002;43:415–24.

Papanicolaou WC. Clinical magnetoencephalography and magnetic source imaging. Cambridge, UK; New York: Cambridge University Press; 2009.

Pascual-Marqui RD. Standardized low-resolution brain electromagnetic tomography (sLORETA): technical details. Methods Find Exp Clin Pharmacol 2002;24:5-12–12. Suppl D.

Penfield W, Jasper HH. Epilepsy and the functional anatomy of the human brain. Boston: Little, Brown; 1954.

Sakamoto S, Tanaka H, Tsuyuguchi N, Terakawa Y, Ohata K, Inoue Y, et al. Quantitative imaging of spontaneous neuromagnetic activity for assessing cerebral ischemia using sLORETA-qm. Neuroimage 2010;49:488–97.

Sakamoto S, Tsuyuguchi N, Takami T, Morino M, Goto T, Hattori H, et al. Interictal patterns of cerebral glucose metabolism, perfusion, and magnetic field in mesial temporal lobe epilepsy. Epilepsia 2003;44:1196–206.

Scherg M, Von Cramon D. Evoked dipole source potentials of the human auditory cortex. Electroencephalogr Clin Neurophysiol 1986;65:344–60.

Sekihara K, Nagarajan SS. Adaptive spatial filters for electromagnetic brain imaging. Berlin: Springer; 2008.

Sekihara K, Sahani M, Nagarajan SS. Localization bias and spatial resolution of adaptive and non-adaptive spatial filters for MEG source reconstruction. Neuroimage 2005;25:1056–67.

Terakawa Y, Tsuyuguchi N, Tanaka H, Shigihara Y, Sakamoto S, Takami T, et al. Quantitative analysis of MEG using modified sLORETA for clinical application. Clin Neurophysiol 2008;119:1917–22.

Wagner M, Fuchs M, Kastner J. Evaluation of sLORETA in the presence of noise and multiple sources. Brain Topogr 2004;16:277–80.